CMI

www.nature.com/cmi

ARTICLE

Mapping the holonomic signaling network that drives pathological changes in endotoxic shock

Teng Teng[1,4], Xinhe Gao[1,4], Peipei Zhang[1], Ye-Hsuan Sun[1], Yifei Liu[1], Rui Zhao[1], Yilong Fu[1], Yiyuan Liu[1], Zhizhong Lin[1], Yingying Zhang[1] and Jiahuai Han[1,2,3]✉

Bacterial lipopolysaccharide (LPS) is among the most potent pathogen-associated molecular patterns (PAMPs). In animals, LPS can induce endotoxic shock, a widely used model of sepsis. Studies of this system have yielded important insights into innate immunity, including key immune sensors and signaling pathways. However, how inflammatory pathways are spatially coordinated across cell types and organs in vivo during endotoxic shock remains poorly understood. Here, we systematically analyzed LPS-induced lethality in mice to define the coordinated contributions of cell death pathways, inflammatory cytokines, and lipid mediators to endotoxic shock pathology. We found that caspase-11 signaling acts primarily in nonhematopoietic cells and drives tissue injury, whereas caspase-8 and RIPK3 function predominantly in hematopoietic cells and are both controlled by TRIF. Although proinflammatory cytokines are thought to promote cell death, it is surprising that cell death and/or components of death signaling are critical for initiating the cytokine storm because disruption of these cell death pathways markedly and preferentially reduces LPS-induced cytokine production in vivo. Combined deficiency of caspase-11, RIPK3, and caspase-8 fully protected mice from LPS-induced death, and additional cyclooxygenase inhibition eliminated remaining sickness behaviors such as reduced mobility. Together, these interventions rendered LPS-treated mice nearly indistinguishable from healthy controls. Overall, we delineate the core of the integrated signaling network that governs the pathological manifestations of LPS-induced endotoxic shock in mice.

Keywords: lipopolysaccharide; endotoxic shock; programmed cell death; cyclooxygenase; cytokines

Cellular & Molecular Immunology; https://doi.org/10.1038/s41423-026-01427-6

INTRODUCTION

For more than 130 years, endotoxin has been regarded as a key determinant of the pathogenicity of Gram-negative bacteria [1]. Chemically, endotoxin is lipopolysaccharide (LPS), one of the most abundant components of the outer membrane of Gram-negative bacteria, and is essential for bacterial survival and proliferation [2]. Toll-like receptor 4 (TLR4), an evolutionarily conserved receptor, serves as the pathogen-associated molecular pattern (PAMP) receptor for LPS [3]. In the presence of lipopolysaccharide-binding protein (LBP) and cluster of differentiation 14 (CD14), LPS activates the TLR4/myeloid differentiation factor 2 (MD-2) complex, which recruits either the myeloid differentiation primary response 88 (MyD88) adaptor complex or the Toll/IL-1 receptor domain-containing adaptor protein inducing interferon-β (TRIF) complex, ultimately activating nuclear factor κB (NF-κB) and mitogen-activated protein kinase (MAPK) signaling [4–9]. The high affinity of LPS for the TLR4 receptor complex enables the activation of target cells at picomolar concentrations. In addition, LPS is sensed intracellularly by caspase-11 in mice (caspase-4/5 in humans), which triggers the noncanonical inflammasome [10–13]. Through these receptors, animals exhibit extreme sensitivity to LPS, making it one of the most potent PAMPs identified to date.

Shortly after Westphal and Lüderitz elucidated the structure of LPS in the 1950s [14], LPS-induced shock (endotoxic shock) in experimental animals became widely used as a prototypical model of septic shock. Endotoxin-challenged mice develop severe hypothermia, weight loss, multiorgan tissue damage, and ultimately death [15]. These outcomes are associated with systemic inflammatory responses, including increased serum levels of multiple inflammatory cytokines [16], which are thought to contribute to lethality. Programmed cell death pathways are also activated during endotoxic shock, and the key mediators of these pathways, such as caspase-11, play important roles in LPS-induced death [10–13]. However, the extent to which targeting these events protects animals from LPS lethality has varied across studies and experimental contexts. A comprehensive view of the signaling network engaged in LPS-challenged mice—and which single or combined interventions can fully prevent lethality—remains lacking.

To define the roles of distinct cell death pathways in endotoxic shock, we systematically analyzed death and inflammatory signaling in LPS-treated mice using highly purified LPS to focus on host responses to LPS. We confirmed that the caspase-11-mediated pyroptosis

[1]State Key Laboratory of Cellular Stress Biology, School of Life Sciences, Faculty of Medicine and Life Sciences, Xiamen University, Fujian, China. [2]Research Unit of Cellular Stress of Chinese Academy of Medical Sciences, Xiang'an Hospital of Xiamen University, Cancer Research Center of Xiamen University, School of Medicine, Faculty of Medicine and Life Sciences, Xiamen University, Fujian, China. [3]Laboratory Animal Center, Faculty of Medicine and Life Sciences, Xiamen University, Fujian, China. [4]These authors contributed equally: Teng Teng, Xinhe Gao. ✉email: jhan@xmu.edu.cn

Received: 14 January 2026 Revised: 9 April 2026 Accepted: 30 April 2026
Published online: 22 May 2026

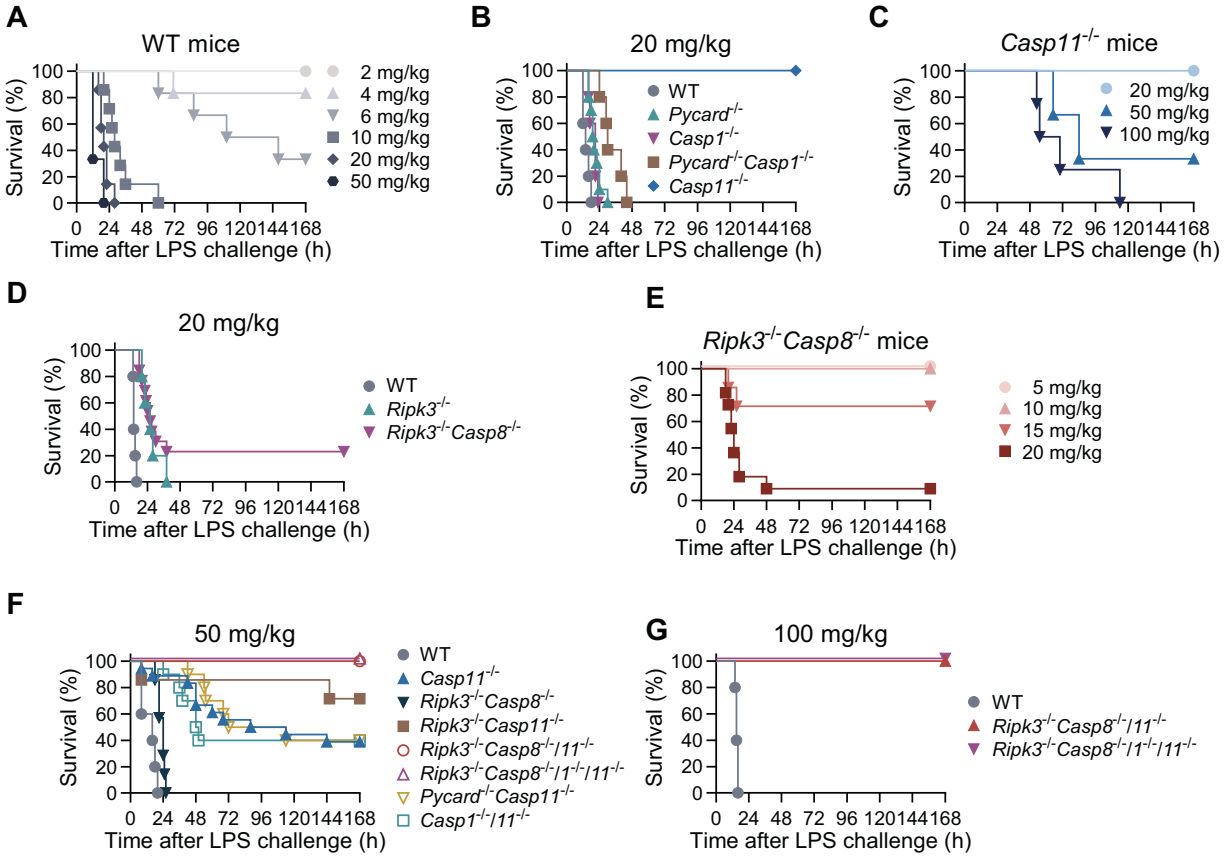

Fig. 1 The pyroptotic, necroptotic, and apoptotic pathways contribute to LPS-induced mouse death. **A** WT mice were injected intraperitoneally (i.p.) with LPS at the indicated doses and monitored for survival. **B**, **D** Mice of the indicated genotypes were injected i.p. with 20 mg/kg LPS and monitored for survival. **C** *Casp11*$^{-/-}$ mice were injected i.p. with LPS at the indicated doses and monitored for survival. **E** *Ripk3*$^{-/-}$ *Casp8*$^{-/-}$ mice were injected i.p. with the indicated doses of LPS, and survival was monitored. **F** Mice of the indicated genotypes were injected i.p. with 50 mg/kg LPS and monitored for survival. **G** Mice of the indicated genotypes were injected i.p. with 100 mg/kg LPS and monitored for survival

pathway is a major driver of LPS-induced lethality and further revealed that it functions predominantly in nonhematopoietic cells, where it contributes substantially to tissue injury. In contrast, receptor-interacting protein kinase 3 (RIPK3)- and caspase-8-dependent necroptotic and apoptotic pathways contribute to LPS-induced lethality primarily through hematopoietic cells. The reciprocal reinforcement between programmed cell death and inflammatory cytokine production was evident: cytokines may promote the induction of key death mediators such as caspase-11, whereas impairment of death pathways markedly blunts cytokine induction in LPS-treated mice. Notably, simultaneous blockade of the RIPK3-, caspase-8-, and caspase-11-mediated pathways fully protected mice from death even at the highest dose of LPS that could be administered. Inflammatory lipid mediators were dispensable for lethality but contributed to sickness behaviors, as cyclooxygenase (COX) inhibition eliminated the remaining LPS-induced clinical signs in *Ripk3*-, *Casp8*-, and *Casp11*-deficient mice. Together, these data provide an integrated map of the signaling pathways that drive sickness behaviors and death in endotoxin-challenged mice.

RESULTS

The contribution of the pyroptotic, necroptotic, and apoptotic pathways to LPS-induced mouse death

Death is the terminal consequence of severe endotoxic shock. Previous studies have shown that disrupting apoptotic, necroptotic, or pyroptotic pathways attenuates LPS-induced lethality in mice [17–21]. For example, LPS-induced cellular responses, tissue damage, and mouse death have been studied in *Casp8*$^{-/-}$*Ripk3*$^{-/-}$ and *Casp11*$^{-/-}$ mice [17]. However, whether these pathways act independently to promote death and whether additional pathway(s) also contribute to lethality after LPS challenge remain unclear. The relationship between the time to death and the dose of highly purified LPS (*E. coli* O111) administered intraperitoneally (i.p.) is shown in Fig. 1A, revealing an LD_{100} of ~10 mg/kg. Disruption of noncanonical inflammasome-dependent pyroptosis via *Casp11* deletion conferred marked resistance to 20 mg/kg LPS challenge. In contrast, disruption of canonical inflammasome-dependent pyroptosis in *Pycard*$^{-/-}$ (ASC), *Casp1*$^{-/-}$, or *Pycard*$^{-/-}$*Casp1*$^{-/-}$ mice had almost no effect on 20 mg/kg LPS-induced death (Fig. 1B). The LD_{100} of *Casp11*$^{-/-}$ mice increased by approximately 10-fold compared with that of wild-type (WT) mice; *Casp11*$^{-/-}$ mice nonetheless died when challenged with 50 mg/kg or higher doses of LPS (Fig. 1C).

We tested the contributions of necroptosis and apoptosis in the same manner. *Ripk3*$^{-/-}$ mice showed a modest increase in resistance. *Ripk3*$^{-/-}$*Casp8*$^{-/-}$ mice exhibited substantially greater resistance, which was consistent with previous work [17] (Fig. 1D). *Ripk3*$^{-/-}$*Casp8*$^{-/-}$ mice were resistant to 10 mg/kg but not 20 mg/kg LPS (Fig. 1E), corresponding to an ~2-fold increase in the LD_{100}.

To determine whether these death pathways act additively or synergistically to drive lethality, we challenged *Casp11*$^{-/-}$, *Ripk3*$^{-/-}$*Casp8*$^{-/-}$, *Pycard*$^{-/-}$*Casp11*$^{-/-}$, *Casp1*$^{-/-}$/*11*$^{-/-}$, *Ripk3*$^{-/-}$*Casp11*$^{-/-}$, *Ripk3*$^{-/-}$*Casp8*$^{-/-}$/*11*$^{-/-}$, and *Ripk3*$^{-/-}$*Casp8*$^{-/-}$/*1*$^{-/-}$/*11*$^{-/-}$ mice with 50 mg/kg LPS (Fig. 1F). Resistance increased as additional pathways were disrupted, with

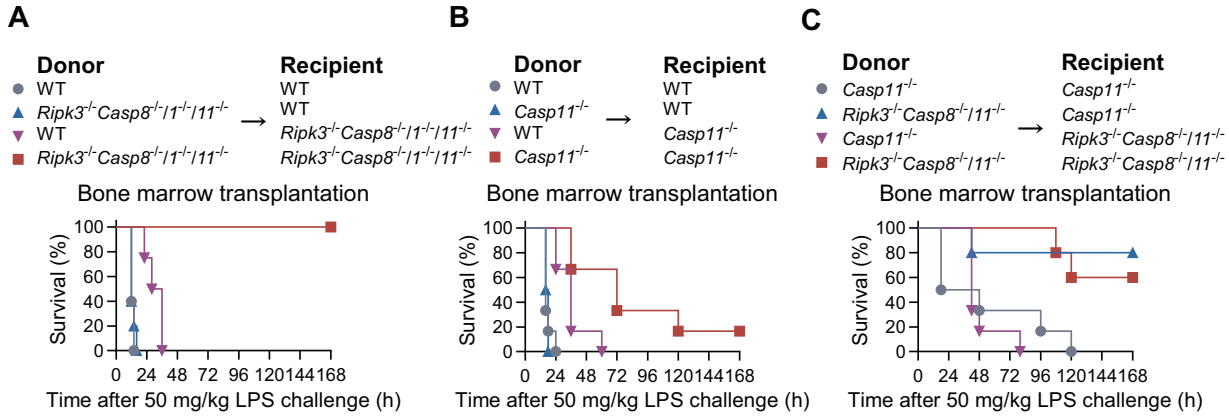

Fig. 2 RIPK3- and caspase-8-dependent pathways function in hematopoietic cells, whereas caspase-11 acts mainly in nonhematopoietic cells. **A–C** Recipient mice were irradiated and transplanted with bone marrow cells from donor mice. The genotypes of the recipient and donor mice are indicated. Following reconstitution, the chimeric mice were injected intraperitoneally (i.p.) with 50 mg/kg LPS and monitored for survival

maximal protection observed when *Casp11*, *Ripk3*, and *Casp8* were deleted simultaneously. Because 100 mg/kg is the highest LPS dose we can administer experimentally, we used this dose as a stringent challenge; *Ripk3*$^{-/-}$*Casp8*$^{-/-}$/*11*$^{-/-}$ and *Ripk3*$^{-/-}$*Casp8*$^{-/-}$/*1*$^{-/-}$/*11*$^{-/-}$ mice survived this challenge (Fig. 1G). These results indicate that these programmed cell death pathways are major determinants of mortality in high-dose LPS-induced murine endotoxic shock.

We also tested LPS from *E. coli* with a distinct O-antigen (O83). O83 LPS was less soluble than O111 LPS was, but both induced TNF-α secretion in a TLR4-dependent manner (Fig. S1A, B). O83 LPS-induced lethality was also fully prevented by the simultaneous disruption of the three death pathways (Fig. S1C). Given that *Casp11* deletion increased the lethal dose by ~10-fold and that combined *Ripk3*/*Casp8* deletion increased it by ~2-fold, the complete survival of mice challenged with 100 mg/kg LPS suggests synergy rather than simple additivity among these pathways.

Deletion of *Casp1*, or additional *Casp1* deletion on *Casp11*$^{-/-}$ or *Ripk3*$^{-/-}$*Casp8*$^{-/-}$/*11*$^{-/-}$ backgrounds, did not increase resistance at LD_{100} doses (Fig. 1B, F), although *Casp1* deficiency may reduce mortality at lower LPS doses [11, 22]. Because *Casp1* and *Casp11* are located on the same chromosome, we obtained some *Casp1*$^{-/-}$/*11*$^{-/-}$ mice and their derivatives through animal cross-breeding. Since caspase-11 has a dominant effect, in subsequent experiments, *Casp1*$^{-/-}$/*11*$^{-/-}$ mice were used primarily as a practical surrogate for *Casp11* deficiency. Because 50 mg/kg *E. coli* O111 LPS challenge overcame the resistance conferred by single-gene deletions, we used 50 mg/kg for most subsequent experiments unless otherwise indicated.

RIPK3 and caspase-8 act in hematopoietic cells, whereas caspase-11 acts predominantly in nonhematopoietic cells

To determine where these pathways function in vivo during LPS-induced lethality, we generated bone marrow chimeras and challenged them with LPS. Deficiency of *Ripk3*, *Casp8*, *Casp1*, and *Casp11* restricted to either hematopoietic or nonhematopoietic compartments alone was insufficient to confer full resistance (Fig. 2A). With respect to *Casp11*, deficiency in nonhematopoietic cells alone provided substantial protection, whereas deficiency restricted to hematopoietic cells had little effect (Fig. 2B). Notably, *Casp11* deficiency in both compartments provided synergistic protection against lethality (Fig. 2B).

Moreover, on a whole-body *Casp11*-deficient background, the deletion of *Ripk3* and *Casp8* in hematopoietic cells—but not in nonhematopoietic cells—further increased protection to a level comparable to that in germline *Ripk3*$^{-/-}$*Casp8*$^{-/-}$/*11*$^{-/-}$ mice (Fig. 2C), indicating that RIPK3 and caspase-8 promote lethality primarily via hematopoietic cells. Given that the resistance of *Ripk3*$^{-/-}$ mice to LPS challenge was limited (Fig. 1D), caspase-8 is likely to play a predominant role in hematopoietic cells.

The slightly lower LPS resistance of *Ripk3*$^{-/-}$*Casp8*$^{-/-}$/*11*$^{-/-}$ mice generated by bone marrow transplantation than of those generated by breeding (Fig. 1F) is likely attributable to the increased fragility sometimes observed in transplanted mice [23]. Nonetheless, these chimera experiments clearly demonstrated that RIPK3 and caspase-8 act mainly in hematopoietic cells, whereas caspase-11 acts predominantly in nonhematopoietic cells during endotoxic shock.

Caspase-11, but not RIPK3 or caspase-8, is involved in LPS-induced tissue/organ damage

To assess how these pathways contribute to endotoxic shock pathology, we examined multiple tissues from LPS-challenged mice. The most prominent histopathological findings were immune cell infiltration in the lung and hemorrhage in the spleen (Fig. 3A–C, Fig. S2). Although overt parenchymal necrosis was not consistently observed in tissue sections, elevated serum AST and ALT levels indicated liver injury (Fig. 3D–E). *Casp11* deficiency largely eliminated these histological changes and prevented the increase in AST and ALT levels after LPS challenge. In contrast, tissue injury in *Ripk3*$^{-/-}$*Casp8*$^{-/-}$ mice was comparable to that in WT mice (Fig. 3A–E). These data indicate that the caspase-11 pathway plays a key role in driving tissue injury during LPS-induced endotoxic shock.

TRIF—RIPK3 and TRIF—caspase-8 axes mediate the loss of hematopoietic cells

At the signaling level, apoptosis, necroptosis, and pyroptosis have been studied extensively in bone marrow-derived macrophages (BMDMs). Consistent with the findings of previous reports, RIPK3-dependent necroptosis in BMDMs can be induced by LPS plus the pancaspase inhibitor zVAD (Fig. S3A–E). This necroptosis is controlled by the TLR4–TRIF–RIPK1/RIPK3 axis [24, 25] (Fig. S3C–K) and is not driven by autocrine TNF-α under these conditions [26] (Fig. S3L, M), although TNF-α-dependent necroptosis can occur in specific contexts; for example, in *Ticam1*-deficient BMDMs, autocrine TNF-α mediates necroptosis, which can be blocked by a TNF-α-neutralizing antibody (Fig. S3N). Although MyD88 is not required to initiate LPS-induced necroptosis, it appears to cooperate with TRIF to enhance the response (Fig. S3I). We noticed that the phosphorylation of RIPK1 also decreased in *Ticam1*$^{-/-}$ cells (Fig. S3K), which could result from an impairment in the assembly of the RIPK1-RIPK3 signaling complex.

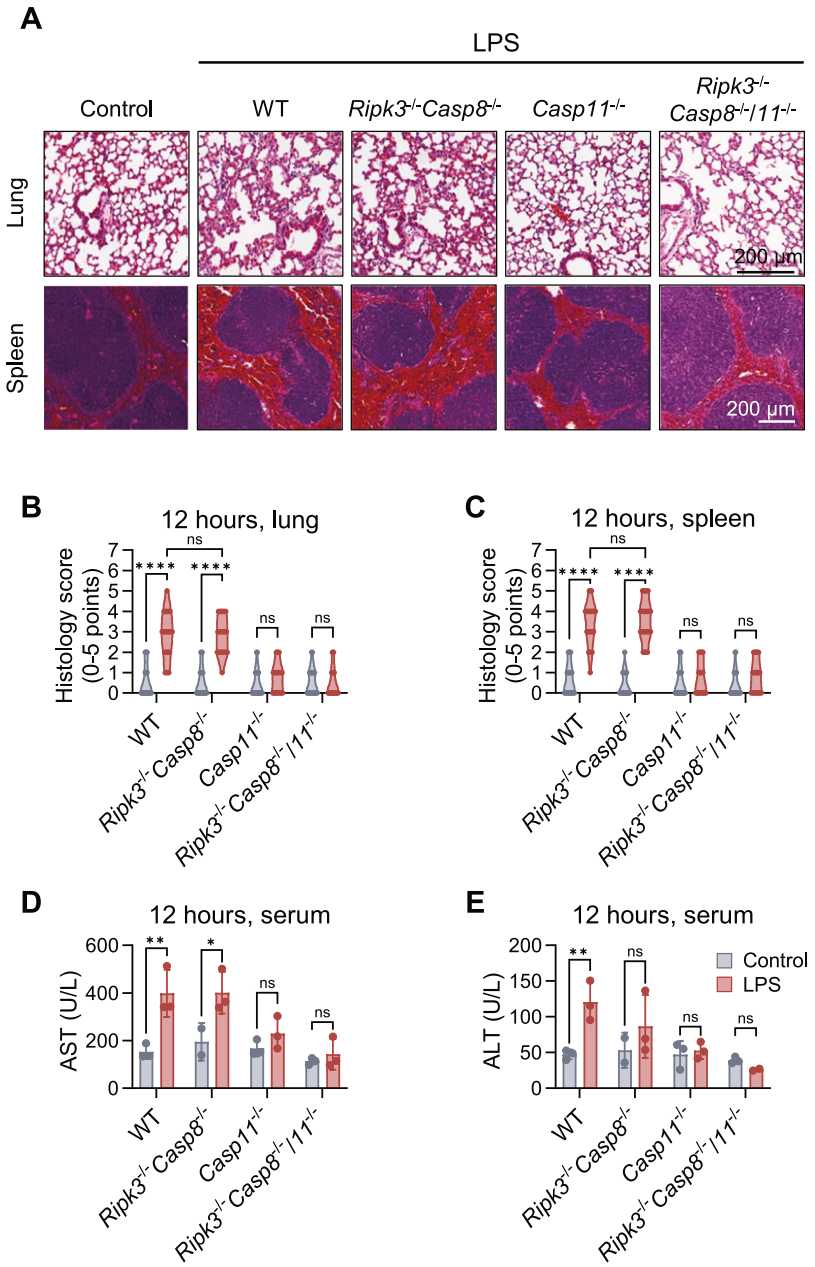

Fig. 3 The caspase-11-dependent pathway determines tissue damage during endotoxic shock. **A**–**E** Mice of the indicated genotypes were injected intraperitoneally (i.p.) with 50 mg/kg LPS. The mice were euthanized 12 h after the challenge, and the tissues and serum were collected. **A** Representative hematoxylin and eosin (H&E)-stained tissue sections are shown. Scale bars, 200 μm. **B**, **C** Quantitative analysis of tissue injury. The tissue sections were scored on a scale of 0–5. 0, no injury; 1-2, mild; 3, moderate; 4, severe; 5, very severe. At least eight fields per sample were evaluated. **D**, **E** Serum AST and ALT levels. *P*-values were calculated using two-way ANOVA. $^{*}P < 0.05$; $^{**}P < 0.01$; $^{****}P < 0.0001$; ns, not significant. The error bars represent the standard deviations (SDs)

Caspase-11-dependent pyroptosis can occur in BMDMs but typically requires cytosolic delivery of LPS [10, 12, 13] (Fig. S4A–C). Canonical inflammasome (NLRP3/caspase-1)-dependent pyroptosis can be induced in BMDMs using a two-signal protocol in vitro [27], but our knockout mouse data indicate that this pathway contributes minimally to lethality in endotoxic shock (Fig. 1B).

With respect to apoptosis, LPS plus a Smac mimetic is typically used to trigger caspase-8-dependent apoptosis in BMDMs [28]. In our experiments, LPS plus the Smac mimetic induced TLR4- and caspase-8-dependent but TNFR1- and caspase-11-independent apoptosis (Fig. S4D–L). Notably, prolonged treatment with a Smac mimetic alone also induced cell death (Fig. S4M, N), which is consistent with reports that Smac mimetics can drive autocrine TNF-α-dependent death under some conditions [29–31].

On the basis of published studies and our aforementioned systematic analysis of BMDMs (Fig. S3, S4), we summarized the LPS-triggered death pathways in Fig. 4A. Given that these pathways may operate in other blood cell types, we predicted that TRIF (*Ticam1*) deletion combined with *Casp11* deletion would prevent lethality after LPS challenge. To test this hypothesis in vivo, we generated *Ticam1*$^{-/-}$*Casp11*$^{-/-}$ mice and challenged them with LPS. *Ticam1*$^{-/-}$*Casp11*$^{-/-}$ mice survived treatment with 50 mg/kg LPS (Fig. 4B), similar to *Ripk3*$^{-/-}$*Casp8*$^{-/-}$/*11*$^{-/-}$ mice (Fig. 1F).

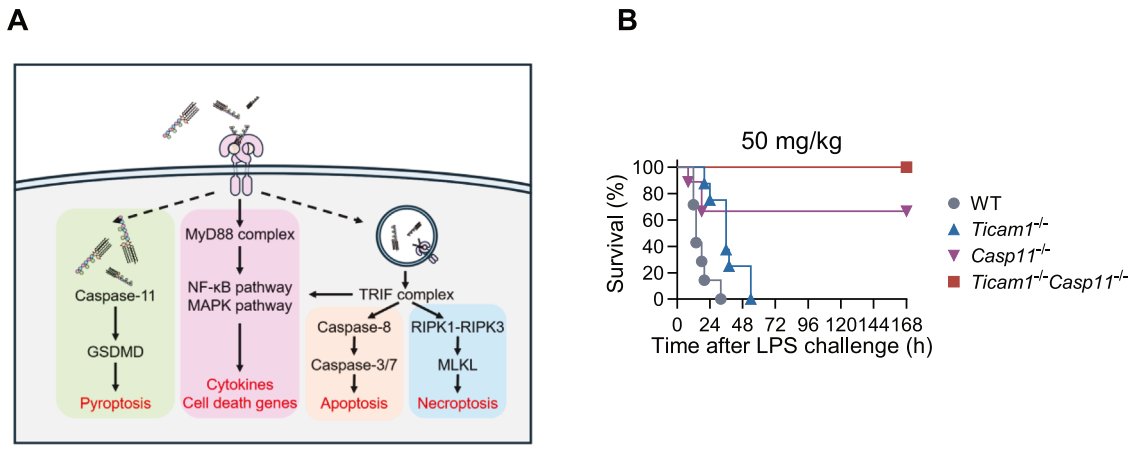

Fig. 4 RIPK3 and caspase-8 are downstream of TRIF. **A** A schematic diagram of LPS-triggered cell death pathways deduced from Fig. S3, S4. **B** Mice of the indicated genotypes were injected i.p. with 50 mg/kg LPS and monitored for survival

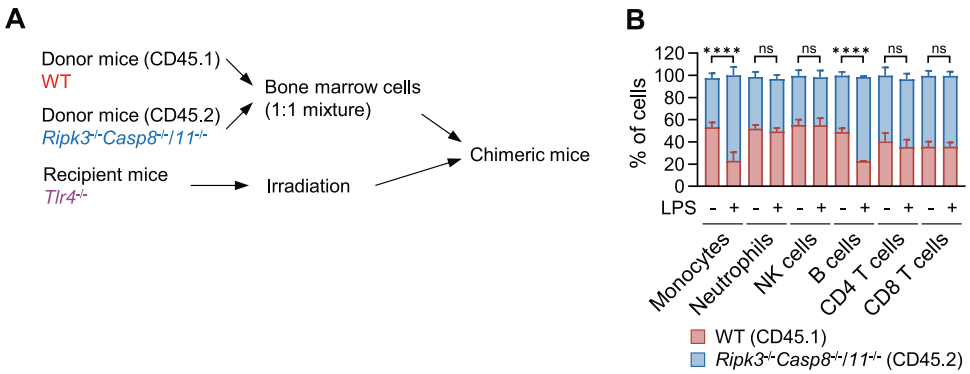

Fig. 5 The function of cell death pathways in hematopoietic cells is linked to cell loss. **A** A schematic diagram illustrating the generation of chimeric mice. **B** Chimeric mice were injected intraperitoneally (i.p.) with 50 mg/kg LPS. Peripheral blood was collected 48 h after the challenge. Monocytes ($CD11b^+Ly\text{-}6C^+$), neutrophils ($CD11b^+Ly\text{-}6G^+$), NK cells ($NK\text{-}1.1^+$), B cells ($B220^+$), CD4 T cells ($CD3^+CD4^+$), and CD8 T cells ($CD3^+CD8^+$) were identified on the basis of surface markers, and the proportions of $CD45.1^+$ and $CD45.2^+$ cells were analyzed among different types of cells. *P*-values were calculated using two-way ANOVA. $^{****}P < 0.0001$; ns, not significant. The error bars represent the standard deviations (SDs)

Since LPS challenge has been reported to reduce lymphocytes, B cells, and erythrocytes in peripheral blood in vivo [32, 33] and because monocytes are particularly susceptible to death during endotoxemia [34], we assessed the contribution of these death pathways in hematopoietic cells in vivo. We generated mixed bone marrow chimeras consisting of CD45.1 WT and CD45.2 $Ripk3^{-/-}Casp8^{-/-}/11^{-/-}$ bone marrow cells transferred into $Tlr4^{-/-}$ recipients (Fig. 5A). In this context, LPS stimulates hematopoietic cells but not nonhematopoietic cells. Flow cytometric analysis of CD45.1 and CD45.2 cells revealed that monocytes and B cells were most strongly preserved by *Ripk3/Casp8/Casp11* deficiency (Fig. 5B), suggesting that these pathways contribute to the loss of circulating monocytes and B cells after LPS challenge.

Collectively, our data suggest that the TRIF–RIPK3 and TRIF–caspase-8 pathways dominate within hematopoietic cells during endotoxic shock and, with possible aid from caspase-11, promote leukocyte loss.

Reciprocal reinforcement between cell death pathways and inflammatory mediators

Inflammatory mediators—including proinflammatory cytokines and lipid mediators—have been implicated in LPS-induced lethality [17, 35–37]. Inhibiting individual mediators (e.g., TNF-α, IL-6, and IL-1β) or cyclooxygenase pathways has been reported to attenuate LPS-induced mortality in some experimental settings. However, whether targeting any single cytokine or lipid pathway can fully prevent death after high-dose LPS challenge remains unclear. For example, the deletion of TNF receptor 1 (TNFR1) increased resistance at lower doses [38] but did not protect against 50 mg/kg LPS in our model (Fig. S5A). Similarly, the COX inhibitor indomethacin did not prevent death after treatment with 50 mg/kg LPS (Fig. S5B), although $Ptgs2^{-/-}$ (COX-2) mice have been reported to resist LD_{50} challenge [35]. These observations suggest that mortality reflects the combined effects of multiple responses, some of which may function in enhancing or amplifying the combined effect under specific conditions.

Because programmed cell death pathways are decisive for lethality in this model (Figs. 1, 2), we next examined how these pathways interact with inflammatory mediators. Although "cytokine storm" is typically defined by rapid systemic increases in the levels of multiple cytokines and chemokines (e.g., TNF-α, IL-6, IL-1β, IFN-γ, and MCP-1), there is no consensus definition for the number or identity of factors needed. While fully "blocking" the cytokine storm is not experimentally feasible, testing whether the inhibition of specific mediators reduces LPS-induced tissue injury in vivo is possible.

Tnfrsf1a deficiency modestly reduced LPS-induced spleen and liver injury, whereas indomethacin only slightly reduced spleen injury (Fig. S5C–G). Together with the results of previous work and our tissue injury analysis (Fig. 3), these findings indicate that among the individual genetic or pharmacologic perturbations

tested, *Casp11* deletion provides the most robust protection against LPS-induced tissue injury.

Caspase-11-mediated pyroptosis requires inducible *Casp11* expression, which can be driven by diverse inflammatory stimuli, including PAMPs, DAMPs, and cytokines [39–41]. Although most mechanistic studies have been performed in immune cells [10–13], caspase-11 induction has been reported across many tissues [42], which is consistent with our finding that caspase-11 acts predominantly in nonhematopoietic cells (Fig. 2B). Thus, inflammatory mediators may promote cell death not only by acutely activating death programs but also by "priming" the system—for example, by inducing caspase-11 expression.

Consistent with widespread cell lysis, serum LDH levels correlated with mortality across the strains examined (Fig. 6A). Similarly, the integrity of death pathways correlated with the release of DAMPs such as histones and HMGB1 into the circulation (Fig. 6B), which would be expected to amplify cytokine production. We therefore measured cytokine levels in LPS-treated mice (Fig. 6C–G). TNF-α and IL-6 induction was significantly reduced by combined *Ripk3*/*Casp8* deletion but was minimally affected by *Casp11* deletion (Fig. 6C–D). IL-1β and IFN-γ levels were reduced by either *Casp11* deletion or *Ripk3*/*Casp8* deletion (Fig. 6E–F). The reduction in MCP-1 levels caused by the blockade of these cell death pathways was moderate and partially additive (Fig. 6G). In addition to indirect effects mediated by DAMP release, components of death pathways may directly modulate cytokine expression. For example, because RIPK3/caspase-8 promotes lethality via hematopoietic cells (Fig. 2C), reduced TNF-α and IL-6 levels in *Ripk3*/*Casp8*-deficient mice may reflect diminished signaling capacity in this compartment. One possible mechanism is that caspase-8 can prolong NF-κB activation via cleavage of NEDD4-binding protein 1 (N4BP1) [43, 44], and cell death itself may further amplify cytokine release. Reduced IL-1β levels in *Casp11*-deficient mice are expected, and the decrease observed in $Ripk3^{-/-}Casp8^{-/-}$ mice may reflect altered NF-κB regulation or secondary effects of reduced cell death. The induction of IFN-γ is slower than that of TNF-α and other early cytokines and may therefore be indirectly reduced because of decreased upstream cytokine signaling [45]. Overall, these data indicate that death pathways profoundly shape systemic cytokine induction in vivo after LPS challenge, both directly and/or indirectly. However, the extent to which reduced cytokine production contributes to survival in $Casp11^{-/-}$, $Ripk3^{-/-}Casp8^{-/-}$, or $Ripk3^{-/-}Casp8^{-/-}/11^{-/-}$ mice remains unresolved.

We also profiled inflammatory lipids and found that circulating PGE_2 was the most strongly induced lipid mediator after LPS challenge; compared with *Casp11* deficiency, lacking *Ripk3* and *Casp8* had a greater effect on PGE_2 suppression (Fig. 6H). Because PGE_2 is largely driven by COX-2 induction, which depends strongly on NF-κB activation [46], these observations are consistent with the cytokine data above. On the basis of these results, we propose a feed-forward circuit in which cell death pathways and inflammatory mediators amplify one another during LPS-induced lethality (Fig. 6I).

Cyclooxygenase signaling drives residual sickness behavior in LPS-treated $Ripk3^{-/-}Casp8^{-/-}/11^{-/-}$ mice

Although simultaneous disruption of caspase-11, RIPK3, and caspase-8 fully protected the mice from LPS-induced death (Fig. 7A), the surviving mice still exhibited sickness behaviors, including hypoactivity, reduced exploratory behavior, and decreased locomotor activity. This differs from $Tlr4^{-/-}$ mice, in which LPS signaling is not initiated. We therefore asked which pathway(s) mediate residual sickness in LPS-treated $Ripk3^{-/-}Casp8^{-/-}/11^{-/-}$ mice.

Cyclooxygenases (COXs) catalyze the conversion of arachidonic acid into prostanoids, including prostaglandins (PGs) [47]. PGE_2 is a potent mediator of inflammation and sickness behavior. COX-1 is constitutively expressed and has been implicated in behavioral changes after nonlethal LPS [48], whereas inducible COX-2 contributes to multiple pathophysiological responses and has been linked to lethality in some settings [35, 49–51]. Notably, intracerebroventricular injection of PGE_2 can recapitulate key behavioral features of LPS-triggered sickness [52].

Consistent with the data shown in Fig. S5B, indomethacin did not prevent death after a 50 mg/kg LPS challenge in WT mice, although it did improve locomotor activity (Fig. 7B). COX inhibition only partially reversed immobility in WT mice (Fig. 7B–E), suggesting that severe tissue injury in high-dose LPS-treated WT mice also directly contributes to sickness behavior.

We next tested whether COX signaling mediated the residual sickness phenotype in 50 mg/kg LPS-treated $Ripk3^{-/-}Casp8^{-/-}/11^{-/-}$ mice by administering indomethacin, as indicated in Fig. 7B. Indomethacin reversed the sickness behaviors described above: mobility recovered to levels comparable to those of $Tlr4^{-/-}$ mice. Open field test (OFT) tracking and associated metrics revealed a broad restoration of locomotor activity (Fig. 7B–D). In the tail suspension test (TST), indomethacin significantly reduced the immobility time of $Ripk3^{-/-}Casp8^{-/-}/11^{-/-}$ mice to a level similar to that of $Tlr4^{-/-}$ mice (Fig. 7E). Although sickness behavior is linked to the development of endotoxic shock, the potential neuroprotective effects of gene deletion or indomethacin treatment in mice might occur.

To define the tissue sources of COX induction, we quantified *Ptgs1* (COX-1) and *Ptgs2* (COX-2) expression across organs by RT–qPCR. The *Ptgs1* expression level decreased after LPS challenge (Fig. 7F), which was also observed in other studies [53, 54]. In contrast, *Ptgs2* expression was strongly induced in the heart, lung, kidney, and brain but only weakly induced in other organs; its induction in the heart and brain was only modestly reduced by *Ripk3*/*Casp8* deletion (Fig. 7G). It is likely that the upregulation of *Ptgs2* affected prostanoid synthesis more than the downregulation of *Ptgs1* did. Additionally, the substrate affinity of COX-2 was reported to be greater than that of COX-1 [55, 56]. Therefore, the overall regulation of *Ptgs2* and *Ptgs1* resulted in the upregulation of prostaglandin (especially PGE_2) production (Fig. 6H). Gene deletion of *Ripk3*/*Casp8*, *Casp11*, or *Ripk3*/*Casp8*/*11* had a minor effect on the changes in the levels of *Ptgs1* and *Ptgs2* induced by LPS (Fig. 7F, G), which is in line with the changes in the circulating PGE_2 level in these different gene-deficient mice (Fig. 6H). Thus, COX signaling is mainly independent of caspase-11/RIPK3/caspase-8 death programs, but some cross-talk is reflected by the partial reduction in the levels of *Ptgs1* and *Ptgs2*, as well as PGE_2, in LPS-treated $Ripk3^{-/-}Casp8^{-/-}/11^{-/-}$ mice. COX-derived prostanoids are primary drivers of sickness behavior when death pathways are disabled.

Collectively, these data show that combined blockade of pyroptosis, necroptosis, and apoptosis, together with inhibition of COX-mediated prostanoid synthesis, provides near-complete protection against both lethality and sickness behavior in murine endotoxic shock. A pathway-level summary is shown in Fig. 8.

DISCUSSION

LPS-induced endotoxic shock largely phenocopies the systemic inflammation, multiorgan damage, and other pathological changes observed in vivo during severe inflammatory diseases. To elucidate the causes of death, we first analyzed how distinct programmed cell death pathways contribute to LPS-induced lethality and mapped where these pathways act in vivo. We then examined the relationships between cell death and inflammatory cytokines and lipid mediators, and we ultimately assessed the contributions of cell death programs and the cyclooxygenase (COX) pathway to sickness behavior. Our data demonstrate that pyroptosis in nonhematopoietic cells, together with apoptosis and necroptosis in hematopoietic cells, is required

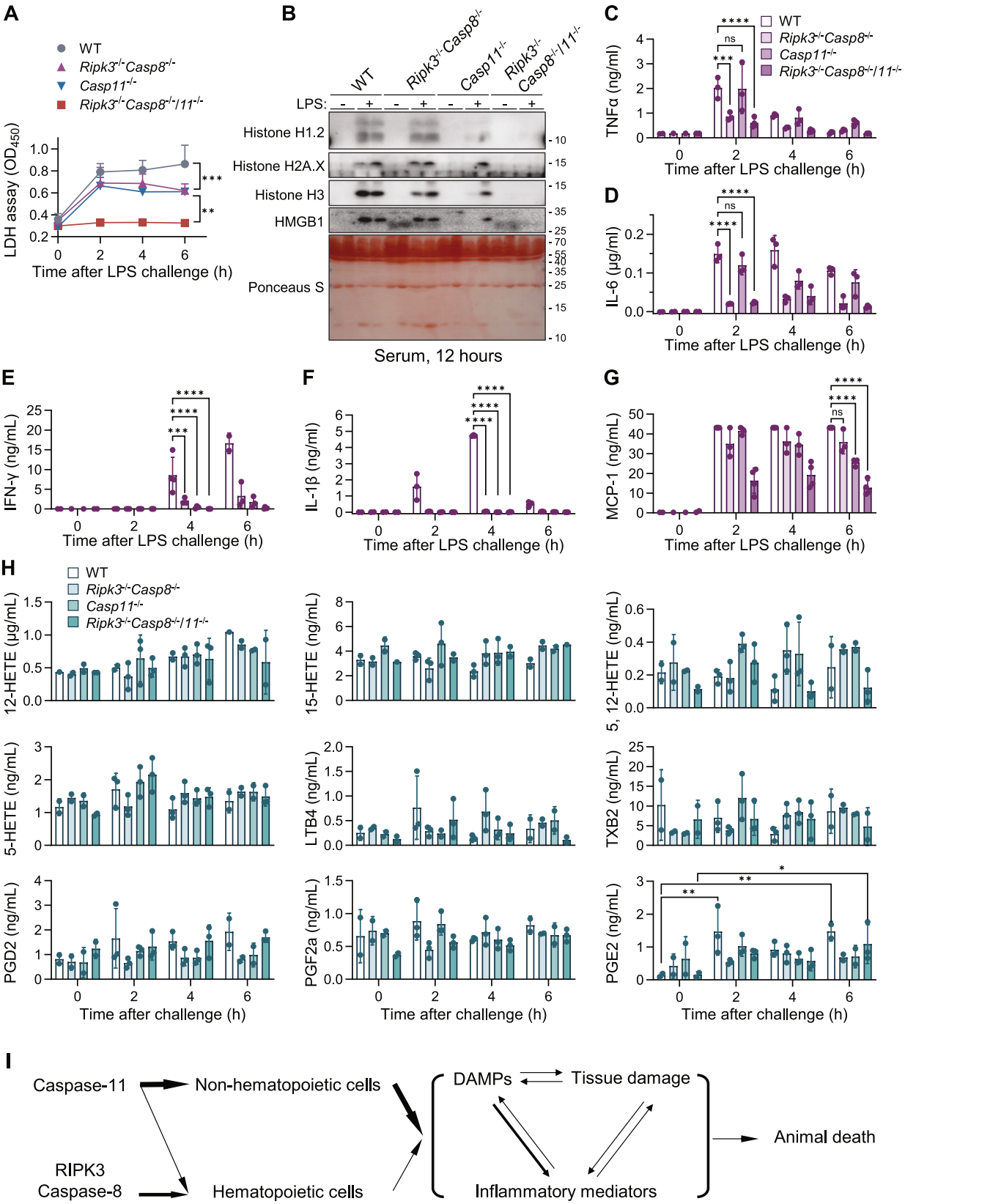

Fig. 6 Cell death pathways and inflammatory mediators mutually reinforce each other. **A**–**H** Mice of the indicated genotypes were injected intraperitoneally (i.p.) with 50 mg/kg LPS. The mice were euthanized, and serum or plasma was collected at the indicated time points after challenge. **A** Relative serum LDH levels (OD_{450}). **B** Serum samples were diluted 1:6 and subjected to Western blot analysis for the indicated DAMPs. Ponceau S staining was used to normalize the protein in serum samples. **C**–**G** Inflammatory cytokine levels. **H** Inflammatory lipid levels. **I** Proposed relationships among pathways and mediators. *P*-values were calculated using two-way ANOVA. $^{*}P < 0.05$; $^{**}P < 0.01$; $^{***}P < 0.001$; $^{****}P < 0.0001$; ns, not significant. The error bars represent the standard deviations (SDs)

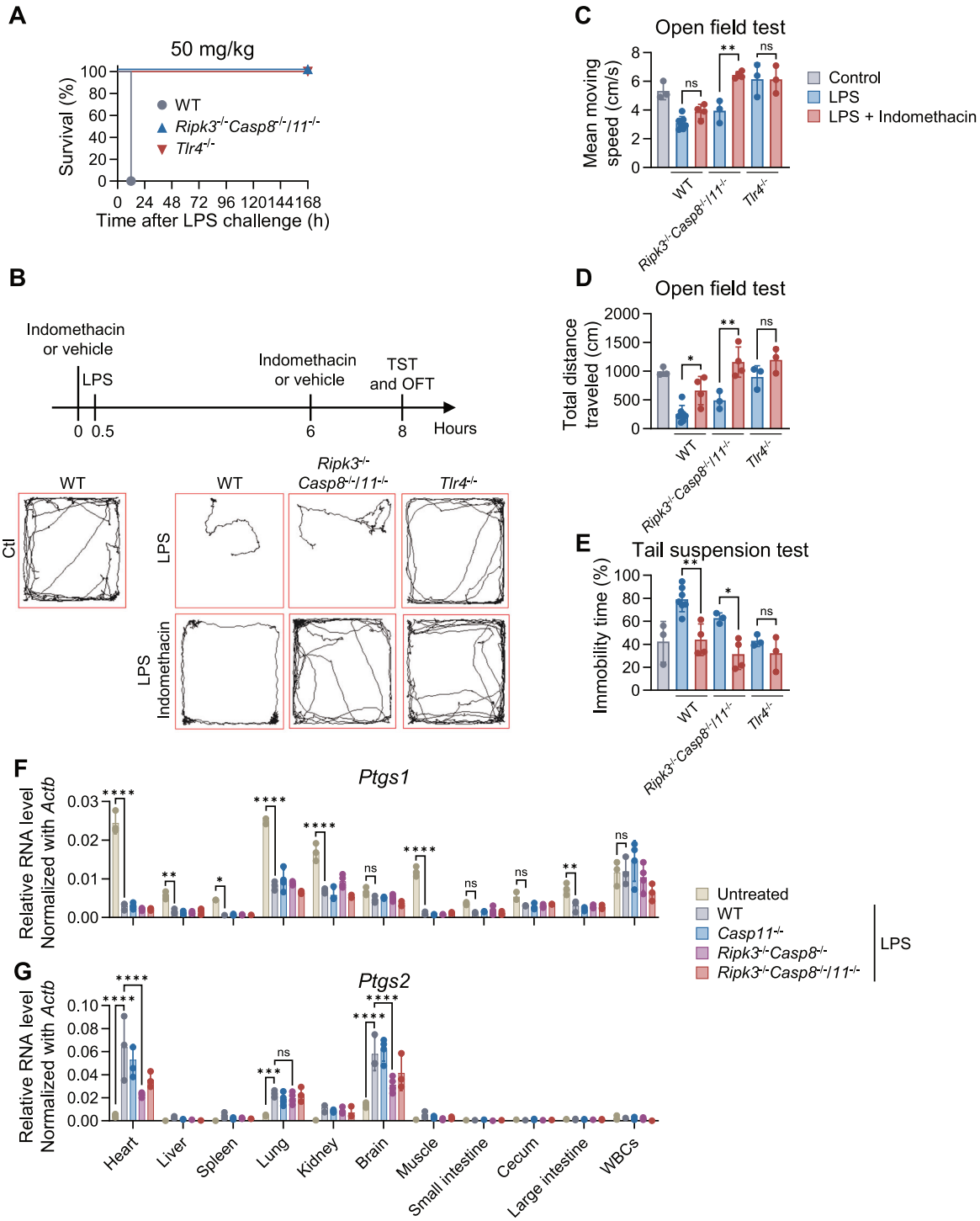

Fig. 7 Residual sickness behavior in LPS-treated *Ripk3*$^{-/-}$*Casp8*$^{-/-}$*/11*$^{-/-}$ mice is mediated by the cyclooxygenase pathway. **A** Mice of the indicated genotypes were injected intraperitoneally (i.p.) with 50 mg/kg LPS and monitored for survival. **B**–**E** Mice received two doses of 15 mg/kg indomethacin (i.p.) and were challenged with 50 mg/kg LPS (i.p.), as schematically illustrated. **B** Schematic illustration of the indomethacin and LPS treatments and representative movement trajectories in the open field test (OFT). **C**, **D** The mean moving speed and total distance traveled in the open field test. **E** Immobility time of mice in the tail suspension test (TST) for 5 min. **F**, **G** Mice of the indicated genotypes were injected i.p. with 50 mg/kg LPS, and tissue samples were collected 4 hours after challenge. The relative mRNA levels of *Ptgs1* (**F**) and *Ptgs2* (**G**) in tissues were measured by RT–qPCR (normalized to *Actb* expression). *P*-values were calculated using two-way ANOVA. **P* < 0.05; ***P* < 0.01; ****P* < 0.001; *****P* < 0.0001; ns, not significant. The error bars represent the standard deviations (SDs)

for LPS-induced death (Figs. 1, 2). Moreover, the production of proinflammatory cytokines and the activation of these cell death pathways are not strictly sequential events; instead, they reciprocally reinforce one another to drive lethality (Fig. 6). Although the COX pathway is not essential for high-dose LPS-induced death, inhibiting COX in combination with blocking major death pathways prevents not only mortality but also sickness behaviors (Fig. 7).

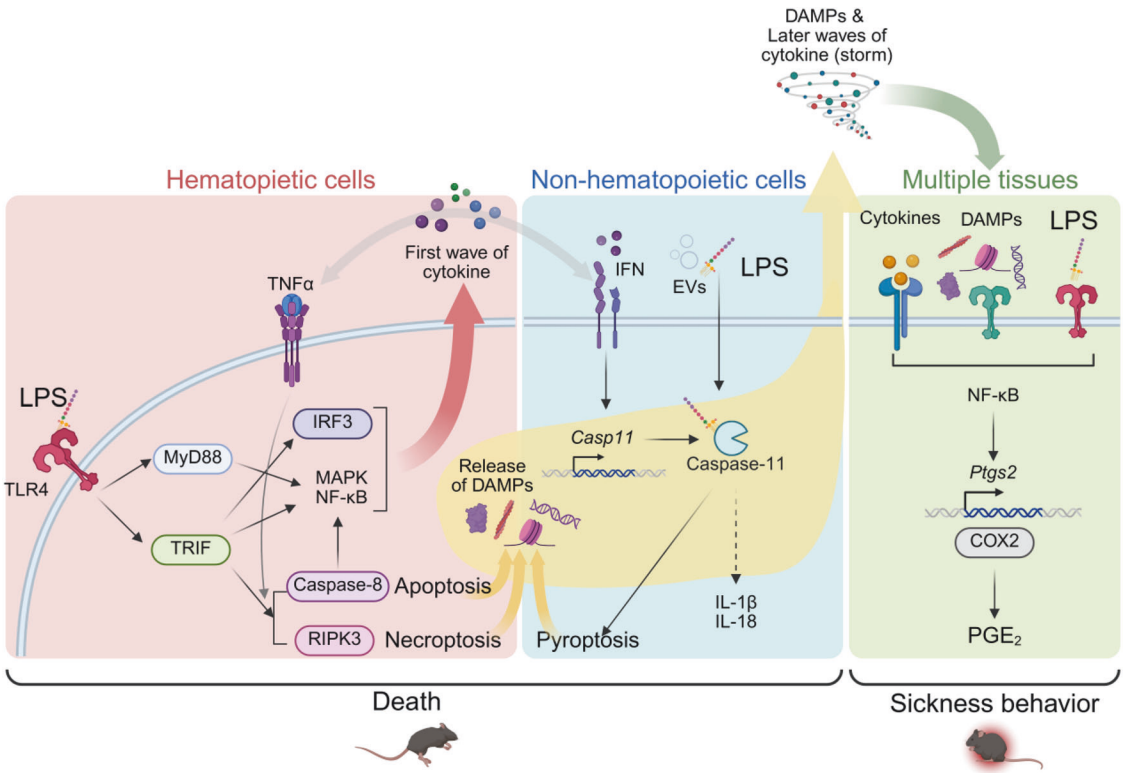

Fig. 8 The signaling network that drives pathological changes in endotoxic shock. Schematic diagram of the roles of cell death and inflammatory pathways in endotoxic shock. The diagram was created in BioRender (https://www.biorender.com/m8vv97i)

The experimental model used here is high-dose, highly purified LPS-induced lethality. We used highly purified LPS because contaminants can activate additional Toll-like receptors, particularly TLR2,which has historically confounded the identification of the LPS receptor [57]. In many settings, commercially available "standard-purity" LPS triggers cellular activation that is not strictly TLR4 dependent [58]. We used a high-dose challenge because our goal was to identify pathways that together are fully responsible for LPS-induced lethality. In addition, rodents, including mice, are more resistant to LPS than humans are [59, 60]. This difference may reflect species-specific differences in the expression and enzymatic activity of murine caspase-11 and human caspase-4; indeed, compared with littermate controls, *CASP4*-transgenic mice are reportedly more sensitive to LPS [61, 62]. Thus, conclusions derived from high-dose LPS challenge in mice might be particularly relevant to LPS-driven septic shock in humans.

Among the death pathways tested, canonical inflammasome-mediated pyroptosis had only a minimal effect on LPS-induced lethality in our model (Fig. 1B). However, at least one published study reported the contribution of canonical inflammasome signaling to LPS-induced death [22]. One explanation is that we used an LD_{100} dose of LPS, whereas the previous study used a lower dose; at high doses, LPS may override the contribution of canonical inflammasome-dependent pyroptosis. A similar explanation may apply to the limited effects of *Tnfrsf1a* deletion or indomethacin treatment in our high-dose model (Fig. S5). There is no doubt that these pathways are activated in endotoxic shock, and their role could involve enhancing or amplifying the main stem signaling in the network that governs the death of LPS-treated mice.

Most prior work on caspase-11-mediated pyroptosis has focused on macrophages [10–13]. In contrast, our results indicate that caspase-11 acts predominantly in nonhematopoietic cells (Fig. 2B) and is responsible for major histological changes and liver injury in LPS-treated mice (Fig. 3), which is consistent with earlier evidence that endothelial caspase-11 can contribute to tissue injury during endotoxic shock [63]. Conversely, although RIPK3 and caspase-8 have often been studied in nonhematopoietic contexts [64–68], our in vivo data show that their contributions to LPS-induced lethality arise primarily from hematopoietic cells (Fig. 2C). Using mixed bone marrow chimeras, we found that monocytes—and unexpectedly, B cells—were major contributors to the decline in circulating hematopoietic cells in endotoxin-shocked mice (Fig. 5). We note that these compartment-specific roles may be context-dependent and should not be generalized to all inflammatory conditions. Nevertheless, our findings support the broader concept that the activation of distinct cell death programs in vivo can exhibit strong spatial specificity across tissues and cell types.

This study also addresses the complex relationship between programmed cell death and cytokine storm during endotoxic shock. Our data support the existence of amplification cycles, driven by bidirectional cross-talk between death pathways and cytokine networks (Fig. 6). When LPS is recognized by the host, proinflammatory cytokines are produced as part of the first-wave response. The impaired production of TNF-α and IL-6 in *Ripk3*$^{-/-}$*Casp8*$^{-/-}$ mice (Fig. 6C, D) may be partially related to the effect of caspase-8 on NF-κB activation [43, 44], but the major cause is most likely the impairment of hematopoietic cell death, which triggers later waves of TNF-α and IL-6 production [69]. Defects in IL-1β induction in *Casp11*$^{-/-}$, *Casp1*$^{-/-}$ and *Ripk3*$^{-/-}$*Casp8*$^{-/-}$ mice have been reported previously [45, 70, 71] (Fig. 6F). These findings indicate that caspase-11 acts via caspase-1 to process pro-IL-1β and that caspase-11-mediated pyroptosis contributes to the release of IL-1β into the circulation. In addition, IL-1β mRNA induction by LPS was impaired in *Ripk3*$^{-/-}$*Casp8*$^{-/-}$ mice. NK and T cells are known to be the major sources of IFN-γ, and the induction of IFN-γ occurs with slower kinetics (Fig. 6E); thus, the impaired IFN-γ induction in these gene deletion mice could be a sequential consequence of NK and T cells, which respond to the

first wave of other proinflammatory cytokines. The first wave of proinflammatory cytokines can trigger later waves of cytokines. They, as well as LPS, can also sensitize cells to death pathways, since the expression of the pyroptosis mediator caspase-11 can be induced by cytokines, including IFNs, TNF-α, and IL-1, in several in vitro models [39–41, 72]. In the model proposed here, both the existing cytokines and the DAMPs released from cell death could amplify inflammatory responses in vivo by promoting both cytokine production and cell death (Fig. 8).

According to Mandal et al., the secretion of TNF-α and type I IFNs contributes to the coordinated activation of caspase-8 and caspase-11 in intestinal epithelial cells, thereby promoting endotoxic shock [17]. Here, we reported that the lung and spleen were the primary organs showing histological damage after LPS challenge (Fig. 3A–C), whereas intestinal damage was limited. In our experiments, *Tnfrsf1a*$^{-/-}$ mice were not resistant to high-dose LPS challenge (Fig. S5A), whereas Mandal et al. reported that a TNF-α-neutralizing antibody can rescue mice from lethal endotoxic shock. In contrast to the full protection against LPS-induced death induced by the genetic deletion of *Casp8* and *Ripk3* reported by Mandal et al. [17], we observed only partial protection in *Casp8*$^{-/-}$*Ripk3*$^{-/-}$ mice. Given that intestinal tissues are major targets of damage during TNF-α-induced SIRS [73–75] and that RIPK3 and caspase-8 are essential components of the TNF-α signaling pathway, the differences between these studies could result from the purity of the LPS used and/or the rearing conditions of the animals, which could lead to different levels of involvement of the TNF-α signaling pathway in endotoxic shock. An important piece of information provided by this study is that the effects of *Casp8* and *Ripk3* deletion predominantly rely on hematopoietic cells rather than intestinal epithelial cells. A framework proposed by Mandal et al. suggests that through the IRF3-IFN axis, caspase-11 is induced, which is the precondition for caspase-11 to play a dominant role in LPS-induced mouse death. Similar studies, including the protective effects observed in *Ripk3*$^{-/-}$ mice in models of low-dose LPS challenge, TNF-α treatment, or lethal polymicrobial sepsis [74, 76], also help to refine our working model (Fig. 8).

In summary, simultaneous blockade of caspase-11-, caspase-8-, and RIPK3-mediated pathways completely protected mice from high-dose LPS-induced death, and additional COX inhibition eliminated the remaining sickness behaviors of endotoxic shock. Together, these four pathways constitute the core of the main signaling network governing endotoxic shock pathology in mice.

MATERIALS AND METHODS

Extraction and purification of lipopolysaccharide

LPS from the *E. coli* O111:B4 strain was extracted using the hot-phenol-water method [77].

Briefly, *E. coli* was cultured in LB medium at 37 °C with shaking at 200 rpm overnight. The bacterial cells were harvested by centrifugation and washed once with physiological saline to remove residual medium. The bacterial pellet was resuspended in saline at a ratio of 2 mL per gram of wet weight. The mixture was heated to 68 °C, and an equal volume of hot phenol was added with vigorous stirring. The mixture was maintained at 68 °C with stirring for 1 h. After cooling on ice, the mixture was centrifuged at 12,000 × g for 15 min at 4 °C. The aqueous phase was collected, and the phenol phase was re-extracted with an equal volume of saline. The aqueous phases were combined and centrifuged again to remove the remaining phenol phase.

The aqueous phase was dialyzed against deionized water using a 3500 Da molecular weight cutoff membrane until residual phenol was removed. $MgCl_2$ was added to a final concentration of 5 mM, followed by the addition of excess DNase and RNase and subsequently proteinase K. Sodium acetate was added to a final concentration of 20 mM, and the sample was subjected to ultracentrifugation at 200,000 × g for 2 h at 4 °C. The resulting pellet was resuspended in double-distilled water and lyophilized to obtain a crude LPS preparation.

LPS from the *E. coli* O83 strain was extracted using the phenol–chloroform–petroleum ether (PCP) method [78].

Briefly, bacterial cells were harvested and sequentially washed with 1% phenol, double-distilled water, ethanol, acetone, and petroleum ether. After drying, 50 g of bacteria was resuspended in 200 mL of extraction solution consisting of 90% phenol, chloroform, and petroleum ether (2:5:8, v/v/v) and homogenized. The suspension was subsequently centrifuged at 5000 × g for 15 min at 4 °C, after which the supernatant was collected. The extraction was repeated twice, and the supernatants were combined and concentrated by rotary evaporation at 60 °C to remove organic solvents. The remaining phenol phase containing LPS was mixed with 0.1 volume of double-distilled water and centrifuged at 3000 × g for 10 min to pellet the LPS. The pellet was subsequently washed three times with 80% phenol and three times with acetone, dried overnight, resuspended in double-distilled water, and subjected to ultracentrifugation at 200,000 × g for 2 h at 4 °C. The resulting pellet was resuspended in double-distilled water and lyophilized to obtain a crude LPS preparation.

Both extracted LPS preparations were purified using the triethylamine-deoxycholate (TEA-DOC) method [57] to minimize TLR4-independent contaminants.

Crude LPS was dissolved in extraction solution (0.2% TEA and 0.5% DOC in double-distilled water) at a ratio of 0.2 mL per mg of crude material and heated to 65 °C to ensure complete dissolution. Half the volume of water-saturated phenol was added, followed by vigorous vortexing for 5 min. The mixture was incubated at room temperature for 5 min and subsequently placed on ice for an additional 5 min. The mixture was subsequently centrifuged at 10,000 × g for 5 min at 4 °C. The aqueous phase was carefully collected, and the phenol phase was re-extracted with an equal volume of extraction solution. The aqueous phases were combined and subjected to repeated extractions with an equal volume of water-saturated phenol until no visible interphase remained. The aqueous phase was collected and centrifuged at 10,000 × g for 5 min at 4 °C again to remove residual phenol. Sodium acetate was added to a final concentration of 30 mM, after which three volumes of ethanol were added, and the samples were incubated at −20 °C overnight to precipitate LPS.

The precipitated LPS was subsequently washed with cold ethanol, dried, resuspended in double-distilled water, and subjected to ultracentrifugation at 200,000 × g for 2 h at 4 °C. The resulting LPS pellet was resuspended in double-distilled water and lyophilized. Lyophilized LPS was dissolved in endotoxin-free PBS or saline at 5 mg/mL and sterilized by filtration.

Protein contamination in the purified LPS was less than 0.5%, as measured by the Pierce BCA protein assay (Thermo Fisher Scientific, 23227). DNA and RNA contamination were each less than 0.5%, as measured by Qubit assays (Thermo Fisher Scientific). The TLR4-dependent activity of the purified LPS was validated experimentally (Fig. S1A, B).

Mice

Ripk3$^{-/-}$, *Casp8*$^{-/-}$, *Casp11*$^{-/-}$, *Tnfrsf1a*$^{-/-}$, *Ticam1*$^{-/-}$, *Pycard*$^{-/-}$, *Gsdmd*$^{-/-}$, and *Casp1*$^{-/-}$*/11*$^{-/-}$ mice were generated as previously described [79, 80]. All cross-genotype mice were produced using IVF technology. For all experiments except bone marrow transplantation, 8- to 12-week-old male littermate mice were used. All mice were on a C57BL/6 J background and housed in a conventional environment under a 12-hour light/dark cycle at the Xiamen University Laboratory Animal Center. All mouse experiments were approved by the Institutional Animal Care and Use Committee and conducted in strict accordance with the good animal practices defined by the Xiamen University Laboratory Animal Center.

In vivo treatments

For the LPS challenge, mice were injected intraperitoneally (i.p.) with 50 mg/kg LPS, unless otherwise indicated. LPS was dissolved in PBS and sterilized by filtration.

For indomethacin treatment, the mice were injected i.p. with 15 mg/kg indomethacin. Indomethacin was administered at 0 h and 6 h, with LPS challenge performed at 0.5 h. Samples were collected at 12 h after the initial indomethacin administration, and the mice were subjected to behavioral tests at 8 h after the initial indomethacin administration. Indomethacin was dissolved in 10% DMSO and 20% sulfobutylether-β-cyclodextrin (SBE-β-CD) in saline for injection. Control mice received the corresponding vehicle.

Bone marrow transplantation

Bone marrow transplantation was performed as previously described [81]. Briefly, 6-week-old recipient mice were irradiated at a dose of 8 Gy. Bone marrow cells from donor mice were intravenously injected into each

recipient mouse 4 h following irradiation. The chimerism of the recipient mice was examined one month later, and the mice were challenged with LPS two months later. To examine chimerism, the ear pinna tissue and peripheral blood leukocytes of mice were collected to extract genomic DNA from nonhematopoietic and hematopoietic cells, respectively. The genotypes of nonhematopoietic and hematopoietic cells were examined by PCR analysis.

Preparation of mouse serum

Peripheral blood was collected from the mice, ensuring that the samples remained free of contamination. For serum preparation, the blood was kept at room temperature for 30 minutes, followed by centrifugation at 2000 × g for 10 min. The supernatant (serum) was carefully collected. Serum was diluted 1:3 with saline, and AST and ALT levels were measured by a chemical analyzer (Mindray, BS-240VET).

H&E staining

The mice were euthanized, and the tissues were collected immediately. The tissues were fixed in 4% paraformaldehyde for 24 h at room temperature. Fixed tissues were dehydrated and embedded in paraffin. The slides were cut into 5 μm sections and stained with hematoxylin–eosin. Slides were analyzed on a Leica Aperio Versa 200 (Leica Biosystems).

Flow cytometry

Peripheral blood samples were collected, and erythrocytes were lysed with ACK buffer (Beyotime, C3702). The cells were subsequently washed and resuspended in FACS buffer (PBS containing 2% FBS). Fc receptors were blocked with a purified rat anti-mouse CD16/CD32 antibody (BD Biosciences, 553141). For surface staining, the cells were incubated with fluorochrome-conjugated antibodies for 30 min at 4 °C. The following antibodies were used: CD45.1 (BioLegend, 110714), CD45.2 (BioLegend, 109830), Ly-6G (BioLegend, 127616), Ly-6C (BioLegend, 128026), NK-1.1 (BioLegend, 108706), CD11b (eBioscience, 12-0112-81), B220 (BioLegend, 103241), CD3 (Thermo Fisher Scientific, 367-0032-80), CD4 (eBioscience, 48-0041-82), and CD8β (BioLegend, 126633). Data were acquired on an ID7000 spectral cell analyzer (Sony).

Tissue RNA extraction and qPCR

The mice were euthanized, and the tissues were collected immediately. The tissues were frozen in liquid nitrogen, and 1.5 ml of RNA extraction reagent (AG RNAex Pro Reagent, Accurate Biotechnology, AG21102) was added to 150 mg of tissue sample. RNA extraction was performed following the manufacturer's instructions. cDNA was synthesized by reverse transcription, and RNA expression was measured by RT–qPCR. RNA expression was normalized to the expression of *Actb*.

The primers for *Ptgs1* were 5′- GATTGTACTCGCACGGGCTAC -3′ and 5′-GGATAAGGTTGGACCGCACT -3′. The primers for *Ptgs2* were 5′-TGTGACTG-TACCCGGACTGG-3′ and 5′-TGCACATTGTAAGTAGGTGGAC-3′. The primers used for *Actb* were 5′-TCCAGCCTTCCTTCTTGGGT-3′ and 5′-GCACTGTGTT GGCATAGAGGT-3′.

Mouse behavioral tests

The mice were subjected to the open field test (OFT) and the tail suspension test (TST). For the open field test, mice were placed in a 40 × 40 cm open field arena and allowed to move freely for 5 min. Locomotor activity and movement trajectories were recorded using the Panlab SMART video tracking system. For the tail suspension test, mice were suspended by the tail and tested for 5 min, during which the immobility time was recorded. All behavioral tests were performed in a dimly lit and quiet environment.

Cell culture and treatments

The generation of BMDMs has been previously described [82]. Bone marrow cells from the tibia and femur of mice were differentiated for 7 days in DMEM supplemented with 10% (v/v) heat-inactivated FBS and 30% L929 conditioned medium. RAW264.7 cells were cultured in DMEM supplemented with 10% (v/v) heat-inactivated FBS. The following reagents were used for cell stimulation: z-VAD-FMK (Calbiochem, 627610), GSK872 (MedChemExpress, HY-101872), LCL-161 (MedChemExpress, HY-15518), a mouse TNF-α-neutralizing antibody (Cell Signaling Technology, 11969S), and an isotype antibody (Invitrogen, 02-6102).

In vitro transfection of LPS

FuGENE 6 transfection reagent (Promega, E2691) was used to transfect LPS into cells in vitro. Before transfection, the BMDMs were primed with 100 ng/mL LPS for 7 h. The transfection mixture was prepared by mixing 0.5 μL of FuGENE 6 transfection reagent and 0.2 μL of 1 mg/mL LPS with 10 μL of FBS-free DMEM. After incubation for 10 min at room temperature, 10 μL per well of the transfection mixture was added to a 96-well culture plate (20 μL per well for a 48-well culture plate). After transfection, LDH release was measured. Cells and culture supernatants were directly mixed with 6× Laemmli sample buffer to generate total culture lysates, which were subsequently subjected to Western blot analysis.

Cytotoxicity assay

Cell death was assessed using the LDH assay with the Cytotoxicity LDH Assay Kit WST (Dojindo Molecular Technologies, CK12). Cell viability was evaluated using the CellTiter-Glo Luminescent Cell Viability Assay (Promega, G7571).

Enzyme-linked immunosorbent assay (ELISA)

The supernatant from cultured cells was diluted 1:6 and assayed for mouse TNF-α by a mouse TNF-α uncoated ELISA kit (Thermo Fisher Scientific, 88-7324-77). Serum samples were assayed using a multiple cytokine ELISA kit (Millipore, MCYTOMAG-70K-06) following the manufacturer's instructions.

Inflammatory lipid analysis

Mouse plasma was collected and immediately transferred to cold methanol for storage at −80 °C. Inflammatory lipids were identified and quantified by AB SCIEX QTRAP-6500 plus. The synthetic standards were purchased from Cayman Chemical.

Western blot

All the samples were collected in Laemmli sample buffer. After brief boiling to denature the proteins, the samples were cooled and loaded onto a Tris–glycine SDS–PAGE gel with an 8–15% acrylamide concentration, depending on the molecular weight of the proteins of interest. Following electrophoresis, the proteins were transferred to a PVDF membrane and blocked with 5% (w/v) BSA in TBST buffer. The membranes were then incubated overnight at 4 °C with diluted primary antibodies on an orbital shaker. After thorough washing, secondary antibodies were applied for 1 hour at room temperature. Following additional wash steps, the membranes were visualized using enhanced chemiluminescence (ECL). The following antibodies were used for Western blotting: histone H1.2 (Proteintech Group, Inc., 19649-1-AP), histone H2A.X (Proteintech Group, Inc., 10856-1-AP), histone H3 (Proteintech Group, Inc., 17168-1-AP), HMGB1 (Abcam, 18255), caspase-11 (Cell Signaling Technology, 14340), GSDMD (Abcam, 209845), RIPK3 (homemade), caspase-8 (Cell Signaling Technology, 4790), RIPK1 (Cell Signaling Technology, 3493), phospho-RIPK1 (Ser166) (Cell Signaling Technology, 31122), phospho-RIPK3 (Thr231/Ser232) (Cell Signaling Technology, 91702), MLKL (homemade), phospho-MLKL (Ser345) (Abcam, 196436), cleaved-caspase-8 (Cell Signaling Technology, 9429), caspase-3 (Cell Signaling Technology, 9662), caspase-7 (Cell Signaling Technology, 9492), PARP (Cell Signaling Technology, 9542), BID (Proteintech Group, Inc., 10988-1-AP), GSDME (Abcam, ab215191), p38α (homemade), phospho-p38α (Cell Signaling Technology, 9211), c-Jun N-terminal kinase (JNK) (Cell Signaling Technology, 9252), phospho-JNK (Thr183/Tyr185) (Cell Signaling Technology, 4668), extracellular signal-related kinase (ERK) (Cell Signaling Technology, 9107), phospho-ERK (Thr202/Tyr204) (Cell Signaling Technology, 4370), IκBα (Cell Signaling Technology, 4812), and glyceraldehyde-3-phosphate dehydrogenase (GAPDH) (Proteintech Group, Inc., 60004-1-Ig). Ponceau S (Sangon, A100860) staining was used to normalize the protein in serum samples.

REFERENCES

1. Pfeiffer R. Weitere untersuchungen über das wesen der choleraimmunität und über specifisch baktericide processe. Z für Hyg und Infektionskrankheiten. 1894;18:1–16.
2. Zhang G, Meredith TC, Kahne D. On the essentiality of lipopolysaccharide to gram-negative bacteria. Curr Opin Microbiol. 2013;16:779–85.
3. Poltorak A, He X, Smirnova I, Liu M-Y, Huffel CV, Du X, et al. Defective LPS signaling in C3H/HeJ and C57BL/10ScCr mice: Mutations in *Tlr4* gene. Science. 1998;282:2085–8.

4. Tobias P, Soldau K, Ulevitch R. Isolation of a lipopolysaccharide-binding acute phase reactant from rabbit serum. J Exp Med. 1986;164:777-93.
5. Wright S, Ramos R, Tobias P, Ulevitch R, Mathison J. CD14, a receptor for complexes of lipopolysaccharide (LPS) and LPS binding protein. Science. 1990;249:1431-3.
6. Shimazu R, Akashi S, Ogata H, Nagai Y, Fukudomr K, Miyake K, et al. MD-2, a molecule that confers lipopolysaccharide responsiveness on Toll-like receptor 4. J Exp Med. 1999;189:1777–82.
7. Wesche H, Henzel W, Shillinglaw W, Li S, Cao Z. MyD88: an adapter that recruits IRAK to the IL-1 receptor complex. Immunity. 1997;7:837–47.
8. Hoebe K, Du X, Georgel P, Janssen E, Tabeta K, Kim SO, et al. Identification of Lps2 as a key transducer of MyD88-independent TIR signaling. Nature. 2003;424:743–8.
9. Yamamoto M, Sato S, Hemmi H, Hoshino K, Kaisho T, Sanjo H, et al. Role of adaptor TRIF in the MyD88-independent Toll-Like receptor signaling pathway. Science. 2003;301:640–3.
10. Shi J, Zhao Y, Wang Y, Gao W, Ding J, Li P, et al. Inflammatory caspases are innate immune receptors for intracellular LPS. Nature. 2014;514:187–92.
11. Kayagaki N, Warming S, Lamkanfi M, Vande Walle L, Louie S, Dong J, et al. Noncanonical inflammasome activation targets caspase-11. Nature. 2011; 479:117–21.
12. Hagar JA, Powell DA, Aachoui Y, Ernst RK, Miao EA. Cytoplasmic LPS activates caspase-11: implications in TLR4-independent endotoxic shock. Science. 2013;341:1250–3.
13. Kayagaki N, Wong MT, Stowe IB, Ramani SR, Gonzalez LC, Akashi-Takamura S, et al. Noncanonical inflammasome activation by intracellular LPS independent of TLR4. Science. 2013;341:1246–9.
14. Westphal O, Luderitz O, Bister F. Über die extraktion von Bakterien mit phenol/ wasser. Z für Naturforsch B: Chem Sci. 1952;7:148–55.
15. Bahrami S, Redl H, Schlag G. Models of endotoxemia in rodents. Schlag G, Redl H, editors. Heidelberg: Springer Berlin; 1993.
16. Beutler B, Milsark IW, Cerami AC. Passive immunization against cachectin/tumor necrosis factor protects mice from lethal effect of endotoxin. Science. 1985;229:869–71.
17. Mandal P, Feng Y, Lyons JD, Berger SB, Otani S, DeLaney A, et al. Caspase-8 collaborates with caspase-11 to drive tissue damage and execution of endotoxic shock. Immunity. 2018;49:42–55.
18. Wang L, Wang T, Li H, Liu Q, Zhang Z, Xie W, et al. Receptor interacting protein 3-mediated necroptosis promotes lipopolysaccharide-induced inflammation and acute respiratory distress syndrome in mice. PLoS One. 2016;11:e0155723.
19. Kayagaki N, Stowe IB, Lee BL, O'Rourke K, Anderson K, Warming S, et al. Caspase-11 cleaves gasdermin D for noncanonical inflammasome signaling. Nature. 2015;526:666–71.
20. Shi J, Zhao Y, Wang K, Shi X, Wang Y, Huang H, et al. Cleavage of GSDMD by inflammatory caspases determines pyroptotic cell death. Nature. 2015;526: 660–5.
21. He WT, Wan H, Hu L, Chen P, Wang X, Huang Z, et al. Gasdermin D is an executor of pyroptosis and required for interleukin-1β secretion. Cell Res. 2015;25:1285–98.
22. Reinke S, Linge M, Diebner HH, Luksch H, Glage S, Gocht A, et al. Noncanonical caspase-1 signaling drives RIP2-dependent and TNF-α-mediated inflammation in vivo. Cell Rep. 2020;30:2501–11.e5.
23. Zhao Y, Zhang J, Han X, Fan S. Total body irradiation induced mouse small intestine senescence as a late effect. J Radiat Res. 2019;60:442–50.
24. Kaiser WJ, Sridharan H, Huang C, Mandal P, Upton JW, Gough PJ, et al. Toll-like receptor 3-mediated necrosis via TRIF, RIP3, and MLKL. J Biol Chem. 2013;288:31268–79.
25. Kim S, Ono K, Han J. Apoptosis by pancaspase inhibitors in lipopolysaccharide-activated macrophages. Am J Physiol-Lung Cell Mol Physiol. 2001;281:L1095-105.
26. He S, Liang Y, Shao F, Wang X. Toll-like receptors activate programmed necrosis in macrophages through a receptor-interacting kinase-3-mediated pathway. Proc Natl Acad Sci. 2011;108:20054–9.
27. Mariathasan S, Weiss DS, Newton K, McBride J, O'Rourke K, Roose-Girma M, et al. Cryopyrin activates the inflammasome in response to toxins and ATP. Nature. 2006;440:228–32.
28. Li L, Thomas R, Suzuki H, Brabander JD, Wang X, Harran P. A small molecule Smac mimic potentiates TRAIL- and TNFα-mediated cell death. Science. 2004; 305:1471–4.
29. Petersen SL, Wang L, Yalcin-Chin A, Li L, Peyton M, Minna J, et al. Autocrine TNFα signaling renders human cancer cells susceptible to Smac-mimetic-induced apoptosis. Cancer Cell. 2007;12:445–56.
30. Lalaoui N, Hanggi K, Brumatti G, Chau D, Nguyen NY, Vasilikos L, et al. Targeting p38 or MK2 enhances the anti-leukemic activity of Smac-mimetics. Cancer Cell. 2016;29:145–58.
31. Han T, Ruan C, Lin H, Zhang Y, Li L, Sun Y-h, et al. RIPK1 S161 phosphorylation promotes further autophosphorylation and cecal necroptosis in TNF-treated mice. J Exp Med. 2025;222:e20250277.
32. Mann M, Mehta A, de Boer CG, Kowalczyk MS, Lee K, Haldeman P, et al. Heterogeneous responses of hematopoietic stem cells to inflammatory stimuli are altered with age. Cell Rep. 2018;25:2992–3005.
33. Bisht K, Tay J, Wellburn RN, McGirr C, Fleming W, Nowlan B, et al. Bacterial lipopolysaccharides suppress erythroblastic islands and erythropoiesis in the bone marrow in an extrinsic and G -CSF-, IL-1-, and TNF-independent manner. Front Immunol. 2020;11:583550.
34. Akiyama M, Kanayama M, Umezawa Y, Nagao T, Izumi Y, Yamamoto M, et al. An early regulatory mechanism of hyperinflammation by restricting monocyte contribution. Front Immunol. 2024;15:1398153.
35. Ejima K, Layne MD, Carvajal IM, Kritek PA, Baron RM, Chen YH, et al. Cyclooxygenase-2-deficient mice are resistant to endotoxin-induced inflammation and death. FASEB J. 2003;17:1325–7.
36. Netea M, Fantuzzi G, Kullberg B, Stuyt R, Pulido E, et al. Neutralization of IL-18 reduces neutrophil tissue accumulation and protects mice against lethal *Escherichia coli* and *Salmonella typhimurium* endotoxemia. J Immunol. 2000;164:2644–9.
37. Marino M, Dunn A, Grail D, Inglese M, Noguchi Y, Richards E, et al. Characterization of tumor necrosis factor-deficient mice. Proc Natl Acad Sci. 1997; 94:8093–8.
38. Van Looveren K, Timmermans S, Vanderhaeghen T, Wallaeys C, Ballegeer M, Souffriau J, et al. Glucocorticoids limit lipopolysaccharide-induced lethal inflammation by a double control system. EMBO Rep. 2020;21:e49762.
39. Man SM, Karki R, Briard B, Burton A, Gingras S, Pelletier S, et al. Differential roles of caspase-1 and caspase-11 in infection and inflammation. Sci Rep. 2017;7:45126.
40. Pollock TY, Vazquez Marrero VR, Brodsky IE, Shin S. TNF licenses macrophages to undergo rapid caspase-1, -11, and -8-mediated cell death that restricts *Legionella pneumophila* infection. Plos Pathog. 2023;19:e1010767.
41. Flood B, Manils J, Nulty C, Flis E, Kenealy S, Barber G, et al. Caspase-11 regulates the tumor suppressor function of STAT1 in a murine model of colitis-associated carcinogenesis. Oncogene. 2019;38:2658–74.
42. Wang S, Miura M, Jung Y, Zhu H, Gagliardini V, Shi L, et al. Identification and characterization of Ich-3, a member of the interleukin-1β converting enzyme (ICE)/Ced-3 family and an upstream regulator of ICE. J Biol Chem. 1996;271:20580–7.
43. Gitlin AD, Heger K, Schubert AF, Reja R, Yan D, Pham VC, et al. Integration of innate immune signaling by caspase-8 cleavage of N4BP1. Nature. 2020; 587:275–80.
44. Shi H, Sun L, Wang Y, Liu A, Zhan X, Li X, et al. N4BP1 negatively regulates NF-κB by binding and inhibiting NEMO oligomerization. Nat Commun. 2021;12:1379.
45. Hochholzer P, Lipford G, Wagner H, Pfeffer K, Heeg K. Role of interleukin-18 (IL-18) during lethal shock: decreased lipopolysaccharide sensitivity but normal superantigen reaction in IL-18-deficient mice. Infect Immun. 2000;68:3502–8.
46. Hwang D, Jang B, Yu G, Boudreau M. Expression of mitogen-inducible cyclooxygenase induced by lipopolysaccharide: mediation through both mitogen-activated protein kinase and NF-κB signaling pathways in macrophages. Biochemical Pharmacol. 1997;54:87–96.
47. Dennis EA, Norris PC. Eicosanoid storm in infection and inflammation. Nat Rev Immunol. 2015;15:511–23.
48. Teeling JL, Cunningham C, Newman TA, Perry VH. The effect of nonsteroidal anti-inflammatory agents on behavioral changes and cytokine production following systemic inflammation: Implications for a role of COX-1. Brain, Behav, Immun. 2010;24:409–19.
49. Engstrom L, Ruud J, Eskilsson A, Larsson A, Mackerlova L, Kugelberg U, et al. Lipopolysaccharide-induced fever depends on prostaglandin E2 production specifically in brain endothelial cells. Endocrinology. 2012;153:4849–61.
50. Li S, Wang Y, Matsumura K, Ballou L, Morham S, Blatteis C. The febrile response to lipopolysaccharide is blocked in cyclooxygenase-$2^{-/-}$, but not in cyclooxygenase-$1^{-/-}$ mice. Brain Res. 1999;825:86–94.
51. Reddy R, Chen G, Tateda K, Tsai W, Phare S, Mancuso P, et al. Selective inhibition of COX-2 improves early survival in murine endotoxemia but not in bacterial peritonitis. Am J Physiol Lung Cell Mol Physiol. 2001;281:L537–43.
52. Kamm GB, Boffi JC, Abd El Hay MY, Rajot D, Cukić A, Havenith MN, et al. Central infusion of prostaglandin E2 reveals a unified representation of sickness in the mouse insular cortex. Biorxiv. 2025.
53. Font-Nieves M, Sans-Fons MG, Gorina R, Bonfill-Teixidor E, Salas-Perdomo A, Marquez-Kisinousky L, et al. Induction of COX-2 enzyme and downregulation of COX-1 expression by lipopolysaccharide (LPS) control prostaglandin E2 production in astrocytes. J Biol Chem. 2012;287:6454–68.
54. Zingarelli B, Southan GJ, Gilad E, O'Connor M, Salzman AL, Szabo C. The inhibitory effects of mercaptoalkylguanidines on cyclo-oxygenase activity. Br J Pharm. 1997;120:357–66.
55. Gierse JK, Hauser SD, Creely DP, Koboldt C, Rangwala SH, Isakson PC, et al. Expression and selective inhibition of the constitutive and inducible forms of human cyclo-oxygenase. Biochem J. 1995;305:479–84.

56. Ruan CH, So SP, Ruan KH. Inducible COX-2 dominates over COX-1 in prostacyclin biosynthesis: mechanisms of COX-2 inhibitor risk to heart disease. Life Sci. 2011;88:24–30.
57. Hirschfeld M, Ma Y, Weis JH, Vogel SN, Weis JJ. Cutting edge: repurification of lipopolysaccharide eliminates signaling through both human and murine toll-like receptor 2. J Immunol. 2000;165:618–22.
58. Parusel R, Steimle A, Lange A, Schafer A, Maerz JK, Bender A, et al. An important question: Which LPS do you use? Virulence. 2017;8:1890–3.
59. Warren HS, Fitting C, Hoff E, Adib-Conquy M, Beasley-Topliffe L, Tesini B, et al. Resilience to bacterial infection: difference between species could be due to proteins in serum. J Infect Dis. 2010;201:223–32.
60. Wichterman KA, Baue AE, Chaudry IH. Sepsis and septic shock—A review of laboratory models and a proposal. J Surgical Res. 1980;29:189–201.
61. Kajiwara Y, Schiff T, Voloudakis G, Gama Sosa MA, Elder G, Bozdagi O, et al. A critical role for human caspase-4 in endotoxin sensitivity. J Immunol. 2014;193:335–43.
62. Wei C, Jiang W, Wang R, Zhong H, He H, Gao X, et al. Brain endothelial GSDMD activation mediates inflammatory BBB breakdown. Nature. 2024;629:893–900.
63. Cheng KT, Xiong S, Ye Z, Hong Z, Di A, Tsang KM, et al. Caspase-11-mediated endothelial pyroptosis underlies endotoxemia-induced lung injury. J Clin Investig. 2017;127:4124–35.
64. Zhang D-W, Shao J, Lin J, Zhang N, Lu B-J, Lin S-C, et al. RIP3, an energy metabolism regulator that switches TNF-induced cell death from apoptosis to necrosis. Science. 2009;325:332–6.
65. He S, Wang L, Miao L, Wang T, Du F, Zhao L, et al. Receptor interacting protein kinase-3 determines cellular necrotic response to TNF-α. Cell. 2009;137:1100–11.
66. Cho YS, Challa S, Moquin D, Genga R, Ray TD, Guildford M, et al. Phosphorylation-driven assembly of the RIP1-RIP3 complex regulates programmed necrosis and virus-induced inflammation. Cell. 2009;137:1112–23.
67. Gunther C, Martini E, Wittkopf N, Amann K, Weigmann B, Neumann H, et al. Caspase-8 regulates TNF-α-induced epithelial necroptosis and terminal ileitis. Nature. 2011;477:335–9.
68. Welz PS, Wullaert A, Vlantis K, Kondylis V, Fernandez-Majada V, Ermolaeva M, et al. FADD prevents RIP3-mediated epithelial cell necrosis and chronic intestinal inflammation. Nature. 2011;477:330–4.
69. Place DE, Kanneganti TD. Cell death-mediated cytokine release and its therapeutic implications. J Exp Med. 2019;216:1474–86.
70. Fantuzzi G, Reed DA, Dinarello CA. IL-12-induced IFN-gamma is dependent on caspase-1 processing of the IL-18 precursor. J Clin Invest. 1999;104:761–7.
71. Philip NH, DeLaney A, Peterson LW, Santos-Marrero M, Grier JT, Sun Y, et al. Activity of Uncleaved Caspase-8 Controls Antibacterial Immune Defense and TLR-Induced Cytokine Production Independent of Cell Death. Plos Pathog. 2016;12:e1005910.
72. Rathinam VA, Vanaja SK, Waggoner L, Sokolovska A, Becker C, Stuart LM, et al. TRIF licenses caspase-11-dependent NLRP3 inflammasome activation by gram-negative bacteria. Cell. 2012;150:606–19.
73. Tracey KJ, Beutler B, Lowry SF, Merryweather J, Wolpe S, Milsark IW, et al. Shock and tissue injury induced by recombinant human cachectin. Science. 1986;234:470–4.
74. Duprez L, Takahashi N, Van Hauwermeiren F, Vandendriessche B, Goossens V, Vanden Berghe T, et al. RIP kinase-dependent necrosis drives lethal systemic inflammatory response syndrome. Immunity. 2011;35:908–18.
75. Wu J, Ai T, He P, Shi Q, Li Y, Zhang Z, et al. Cecal necroptosis triggers lethal cardiac dysfunction in TNF-induced severe SIRS. Cell Rep. 2024;43:114778.
76. Chen H, Li Y, Wu J, Li G, Tao X, Lai K, et al. RIPK3 collaborates with GSDMD to drive tissue injury in lethal polymicrobial sepsis. Cell Death Differ. 2020;27:2568–85.
77. Shnyra A, Luchi M, Morrison DC. Septic shock methods and protocols. Evans TJ, editor: Human press; 2000.
78. Galanos C, Luderitz O, Westphal O. A new method for the extraction of R lipopolysaccharides. Eur J Biochem. 1969;9:245–9.
79. Zhang P, Liu Y, Hu L, Huang K, Hong M, Wang Y, et al. NLRC4 inflammasome–dependent cell death occurs by a complementary series of three death pathways and determines lethality in mice. Sci Adv. 2021;7:eabi9471.
80. Wang R, Li H, Wu J, Cai ZY, Li B, Ni H, et al. Gut stem cell necroptosis by genome instability triggers bowel inflammation. Nature. 2020;580:386–90.
81. Gao X, Teng T, Liu Y, Ai T, Zhao R, Fu Y, et al. Anthrax lethal toxin and tumor necrosis factor-α synergize on intestinal epithelia to induce mouse death. Protein Cell. 2024;15:135–48.
82. Wu X, Yang ZH, Wu J, Han J. Ribosome-rescuer PELO catalyzes the oligomeric assembly of NOD-like receptor family proteins by activating their ATPase enzymatic activity. Immunity. 2023;56:926-43.

ACKNOWLEDGEMENTS

This work was supported by the National Natural Science Foundation of China (82388201 to JH), the Fundamental and Interdisciplinary Disciplines Breakthrough Plan of the Ministry of Education of China (JYB2025XDXM506 to JH), the 111 Project (B25055 to JH), and the CAMS Innovation Fund for Medical Sciences (2019-I2M-5-062 to JH).

AUTHOR CONTRIBUTIONS

TT, XG, PZ, and JH conceived and designed the study. TT and XG performed most of the experiments. TT, XG, PZ, Y-HS, Yifei L, RZ, YF, and Yiyuan L carried out the animal experiments. TT, XG, Yiyuan L, ZL, and YZ analyzed the data. TT, XG, and JH drafted the manuscript. All the authors discussed the results and contributed to the final manuscript. JH supervised the project.

COMPETING INTERESTS

The authors declare no competing interests.

ADDITIONAL INFORMATION

Supplementary information The online version contains supplementary material available at https://doi.org/10.1038/s41423-026-01427-6.

Correspondence and requests for materials should be addressed to Jiahuai Han.

Reprints and permission information is available at http://www.nature.com/reprints

Publisher's note Springer Nature remains neutral with regard to jurisdictional claims in published maps and institutional affiliations.

Figure S1

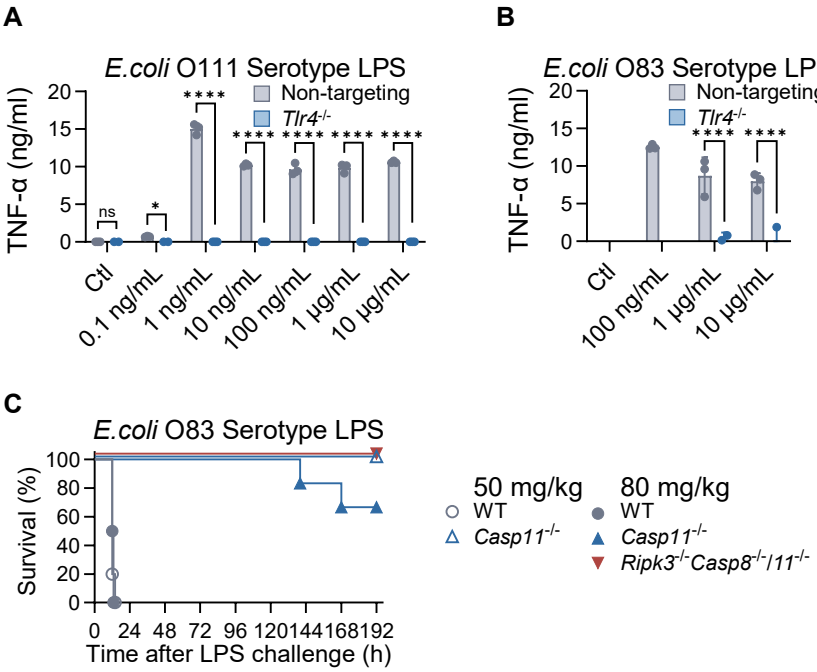
A
E.coli O111 Serotype LPS
Non-targeting
Tlr4-/-
TNF-α (ng/ml)
20
15
10
5
0
ns
*
****
Ctl
0.1 ng/mL
1 ng/mL
10 ng/mL
100 ng/mL
1 μg/mL
10 μg/mL
B
E.coli O83 Serotype LPS
Non-targeting
Tlr4-/-
TNF-α (ng/ml)
****
Ctl
100 ng/mL
1 μg/mL
10 μg/mL
C
E.coli O83 Serotype LPS
Survival (%)
100
80
60
40
20
0
0 24 48 72 96 120 144 168 192
Time after LPS challenge (h)
50 mg/kg
WT
Casp11-/-
80 mg/kg
WT
Casp11-/-
Ripk3-/-Casp8-/-/11-/-

Figure S2

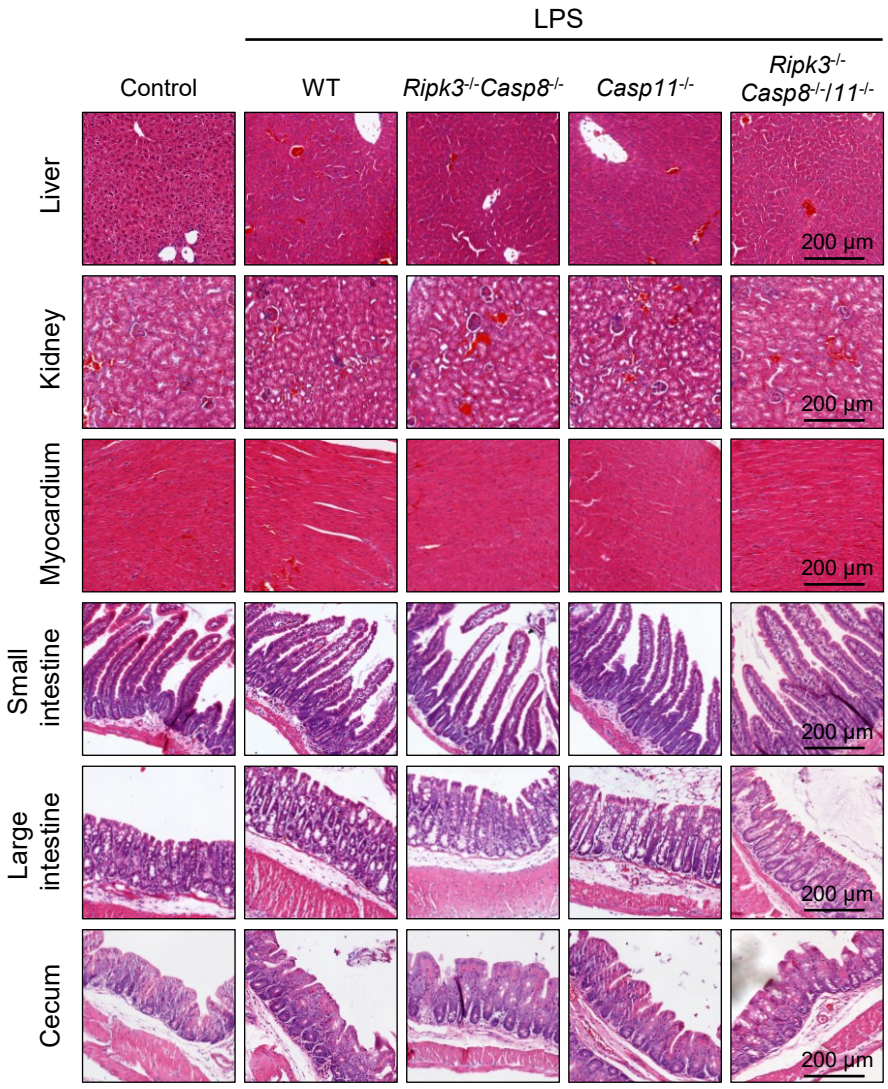
LPS
Control
WT
Ripk3-/-Casp8-/-
Casp11-/-
Ripk3-/-Casp8-/-/11-/-
Liver
Kidney
Myocardium
Small intestine
Large intestine
Cecum
200 μm

Figure S3

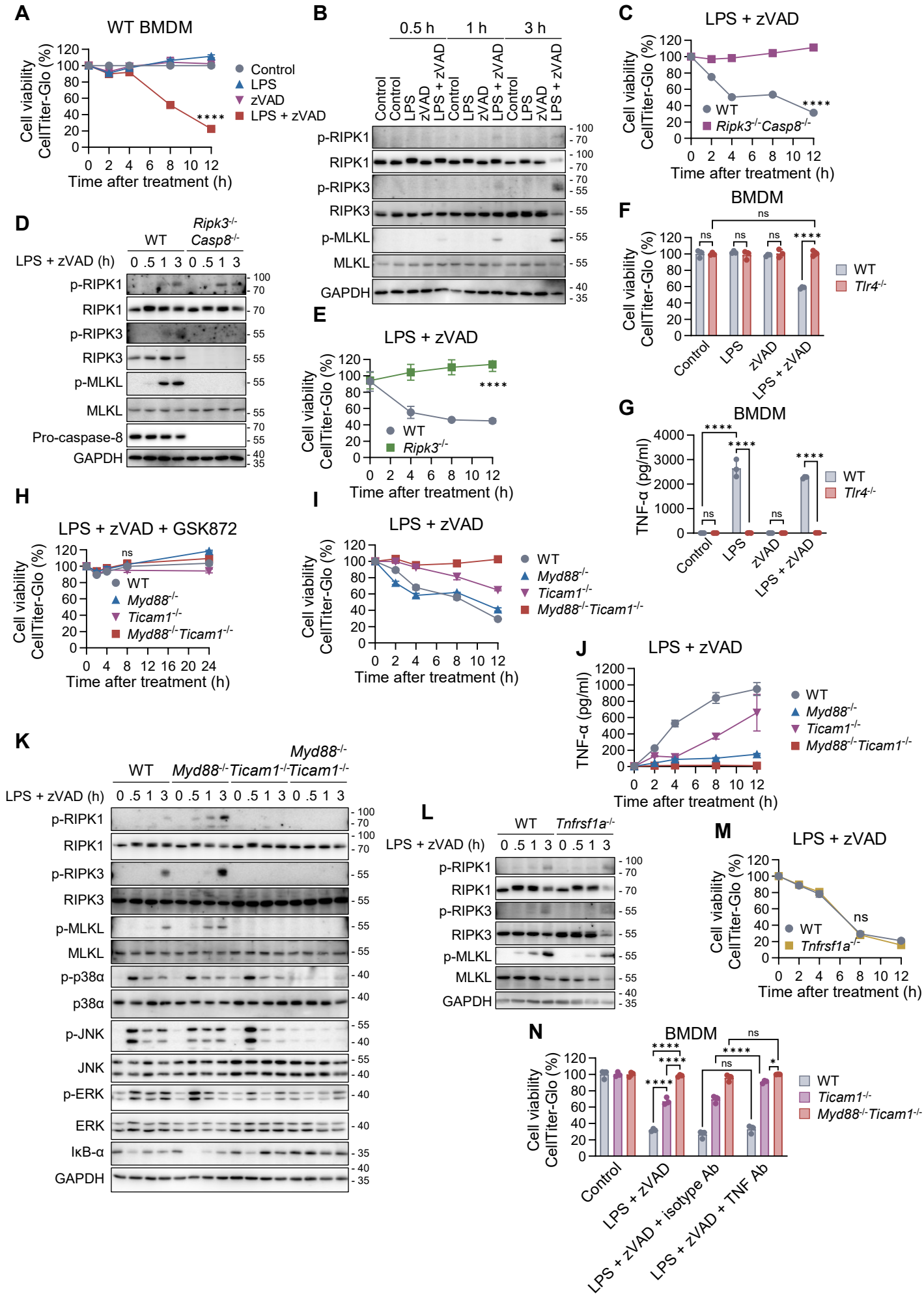
A
WT BMDM
Cell viability CellTiter-Glo (%)
Time after treatment (h)
Control
LPS
zVAD
LPS + zVAD
****
B
0.5 h
1 h
3 h
Control
LPS
zVAD
LPS + zVAD
p-RIPK1
RIPK1
p-RIPK3
RIPK3
p-MLKL
MLKL
GAPDH
C
LPS + zVAD
WT
Ripk3-/-Casp8-/-
D
WT
Ripk3-/- Casp8-/-
LPS + zVAD (h)
Pro-caspase-8
E
LPS + zVAD
WT
Ripk3-/-
F
BMDM
ns
WT
Tlr4-/-
G
BMDM
TNF-α (pg/ml)
H
LPS + zVAD + GSK872
WT
Myd88-/-
Ticam1-/-
Myd88-/-Ticam1-/-
I
LPS + zVAD
J
LPS + zVAD
K
WT
Myd88-/-
Ticam1-/-
Myd88-/- Ticam1-/-
p-p38α
p38α
p-JNK
JNK
p-ERK
ERK
IκB-α
L
WT
Tnfrsf1a-/-
M
LPS + zVAD
N
BMDM
Control
LPS + zVAD
LPS + zVAD + isotype Ab
LPS + zVAD + TNF Ab

Figure S4

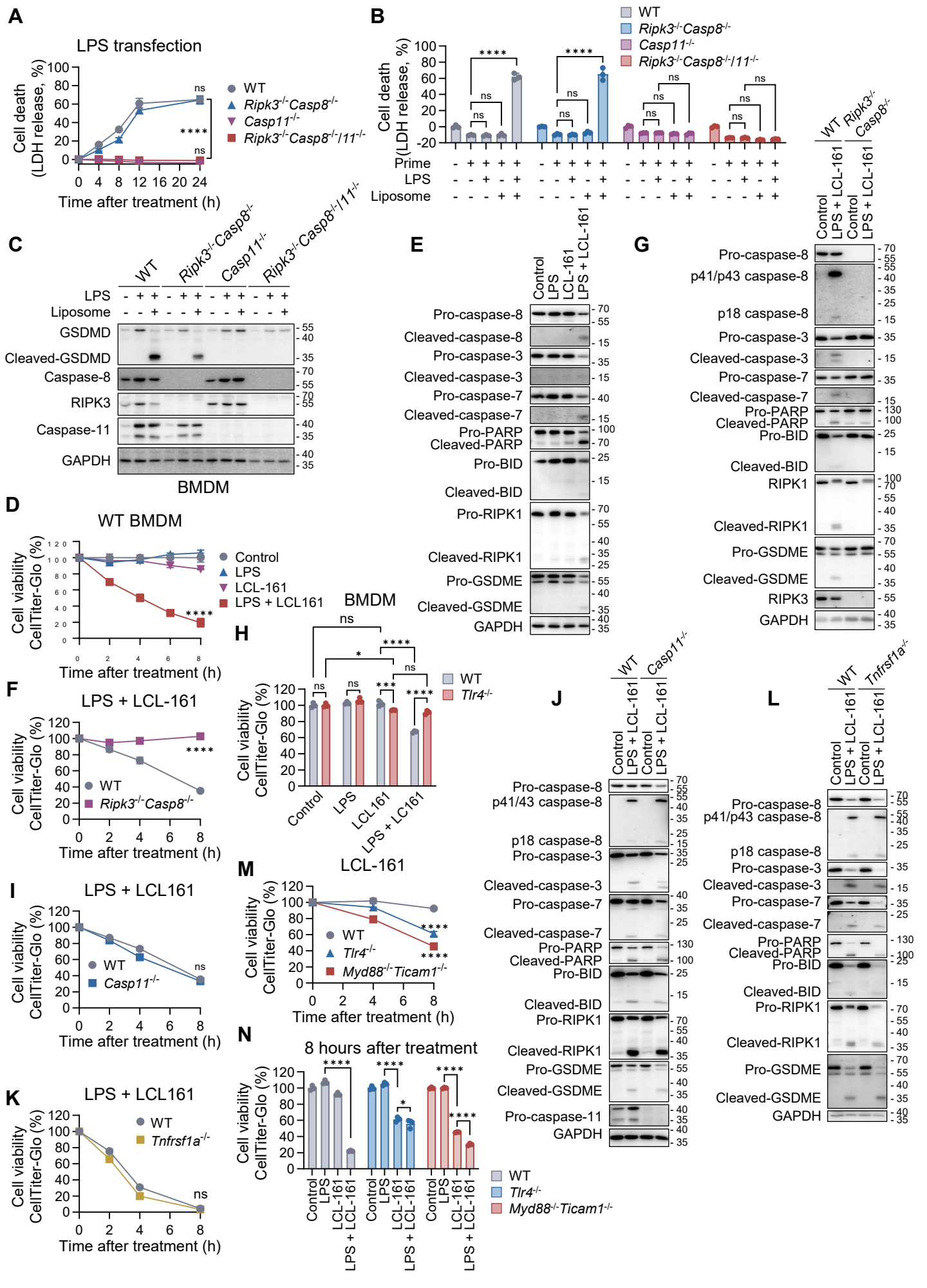
A
LPS transfection
Cell death (LDH release, %)
Time after treatment (h)
WT
Ripk3-/-Casp8-/-
Casp11-/-
Ripk3-/-Casp8-/-/11-/-
B
Cell death (LDH release, %)
WT
Ripk3-/-Casp8-/-
Casp11-/-
Ripk3-/-Casp8-/-/11-/-
Prime
LPS
Liposome
C
WT
Ripk3-/-Casp8-/-
Casp11-/-
Ripk3-/-Casp8-/-/11-/-
LPS
Liposome
GSDMD
Cleaved-GSDMD
Caspase-8
RIPK3
Caspase-11
GAPDH
BMDM
D
WT BMDM
Cell viability CellTiter-Glo (%)
Time after treatment (h)
Control
LPS
LCL-161
LPS + LCL161
E
Control
LPS
LCL-161
LPS + LCL-161
Pro-caspase-8
Cleaved-caspase-8
Pro-caspase-3
Cleaved-caspase-3
Pro-caspase-7
Cleaved-caspase-7
Pro-PARP
Cleaved-PARP
Pro-BID
Cleaved-BID
Pro-RIPK1
Cleaved-RIPK1
Pro-GSDME
Cleaved-GSDME
GAPDH
F
LPS + LCL-161
Cell viability CellTiter-Glo (%)
Time after treatment (h)
WT
Ripk3-/-Casp8-/-
G
WT
Ripk3-/-Casp8-/-
Control
LPS + LCL-161
Pro-caspase-8
p41/p43 caspase-8
p18 caspase-8
Pro-caspase-3
Cleaved-caspase-3
Pro-caspase-7
Cleaved-caspase-7
Pro-PARP
Cleaved-PARP
Pro-BID
Cleaved-BID
RIPK1
Cleaved-RIPK1
Pro-GSDME
Cleaved-GSDME
RIPK3
GAPDH
H
BMDM
Cell viability CellTiter-Glo (%)
WT
Tlr4-/-
Control
LPS
LCL161
LPS + LC161
I
LPS + LCL161
Cell viability CellTiter-Glo (%)
Time after treatment (h)
WT
Casp11-/-
J
WT
Casp11-/-
Control
LPS + LCL-161
Pro-caspase-8
p41/43 caspase-8
p18 caspase-8
Pro-caspase-3
Cleaved-caspase-3
Pro-caspase-7
Cleaved-caspase-7
Pro-PARP
Cleaved-PARP
Pro-BID
Cleaved-BID
Pro-RIPK1
Cleaved-RIPK1
Pro-GSDME
Cleaved-GSDME
Pro-caspase-11
GAPDH
K
LPS + LCL161
Cell viability CellTiter-Glo (%)
Time after treatment (h)
WT
Tnfrsf1a-/-
L
WT
Tnfrsf1a-/-
Control
LPS + LCL-161
Pro-caspase-8
p41/p43 caspase-8
p18 caspase-8
Pro-caspase-3
Cleaved-caspase-3
Pro-caspase-7
Cleaved-caspase-7
Pro-PARP
Cleaved-PARP
Pro-BID
Cleaved-BID
Pro-RIPK1
Cleaved-RIPK1
Pro-GSDME
Cleaved-GSDME
GAPDH
M
LCL-161
Cell viability CellTiter-Glo (%)
Time after treatment (h)
WT
Tlr4-/-
Myd88-/-Ticam1-/-
N
8 hours after treatment
Cell viability CellTiter-Glo (%)
Control
LPS
LCL-161
LPS + LCL-161
WT
Tlr4-/-
Myd88-/-Ticam1-/-

Figure S5

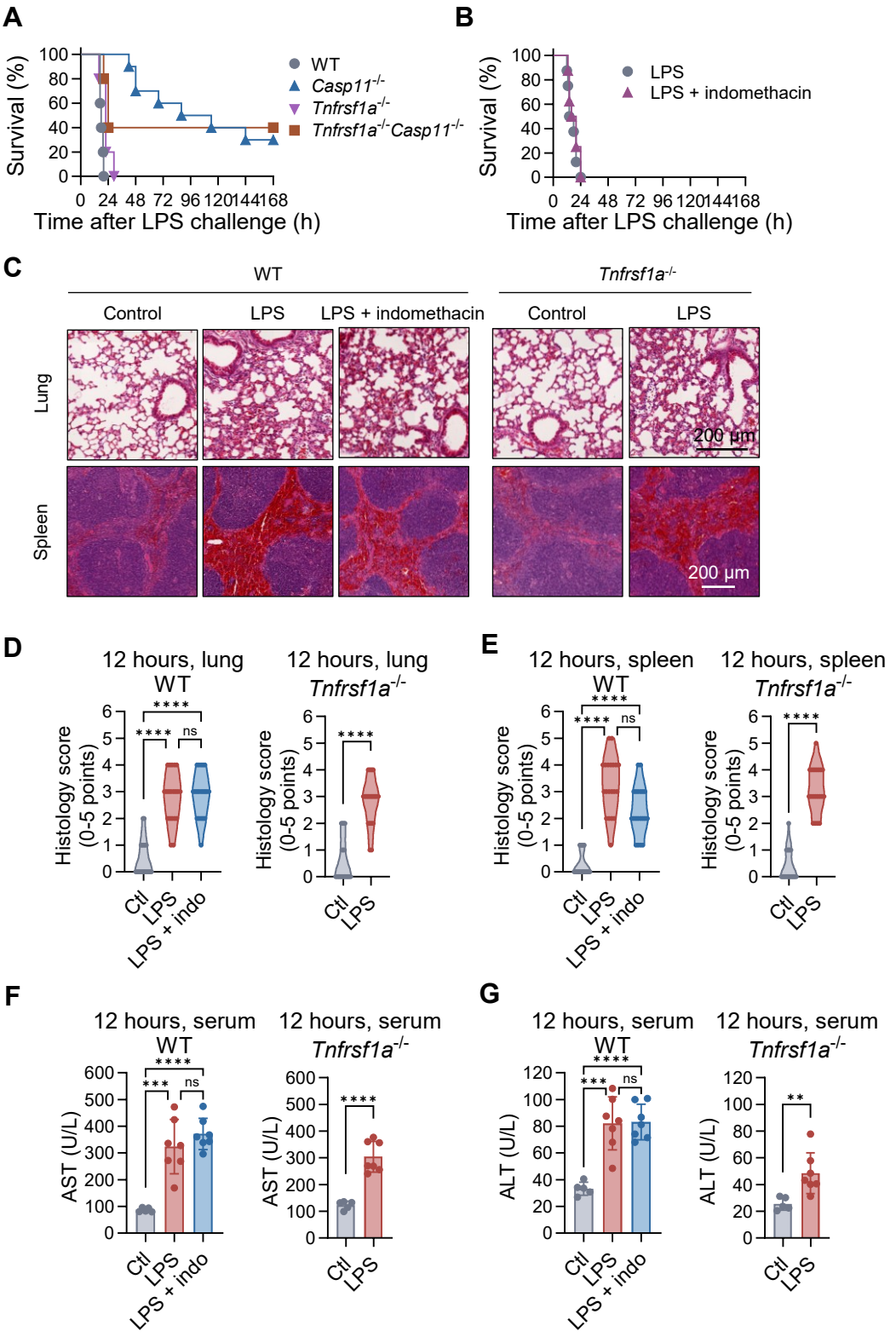
A
Survival (%)
100
80
60
40
20
0
0 24 48 72 96 120 144 168
Time after LPS challenge (h)
WT
Casp11-/-
Tnfrsf1a-/-
Tnfrsf1a-/-Casp11-/-
B
Survival (%)
Time after LPS challenge (h)
LPS
LPS + indomethacin
C
WT
Tnfrsf1a-/-
Control
LPS
LPS + indomethacin
Control
LPS
Lung
Spleen
200 µm
200 µm
D
12 hours, lung
WT
12 hours, lung
Tnfrsf1a-/-
Histology score (0-5 points)
****
ns
Ctl
LPS
LPS + indo
E
12 hours, spleen
WT
12 hours, spleen
Tnfrsf1a-/-
F
12 hours, serum
WT
12 hours, serum
Tnfrsf1a-/-
AST (U/L)
***
G
12 hours, serum
WT
12 hours, serum
Tnfrsf1a-/-
ALT (U/L)
**